UNIVERSITY OF GAZİANTEP

GRADUATE SCHOOL OF

NATURAL & APPLIED SCIENCES

ELASTO-PLASTIC ANALYSIS OF THICK BEAMS

USING MESHFREE METHODS

M.Sc. THESIS

IN

MECHANICAL ENGINEERING

BY

NURETTİN FURKAN DOĞAN

JULY 2015

Elasto-Plastic Analysis of Thick Beams
Using Meshfree Methods

M.Sc. Thesis

in

Mechanical Engineering
University of Gaziantep

Supervisor
Prof. Dr. Bahattin KANBER

By
Nurettin Furkan DOĞAN
July 2015

REPUBLIC OF TURKEY

UNIVERSITY OF GAZİANTEP
GRADUATE SCHOOL OF NATURAL & APPLIED SCIENCES
MECHANICAL ENGINEERING

Name of the thesis: Elasto-Plastic Analysis of Thick Beams Using Meshfree Methods

Name of student   : Nurettin Furkan DOĞAN
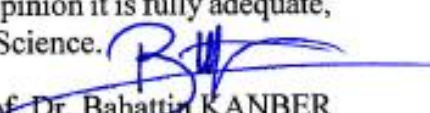
Exam Date   : 03.07.2015

Approval of the Graduate School of Natural and Applied Sciences

Prof. Dr. Metin BEDİR

Director

I certify that this thesis satisfies all the requirements as a thesis for the degree of Master
of Science.

Prof. Dr. M. Sait SÖYLEMEZ

Head of Department

This is to certify that we have read this thesis and that in our opinion it is fully adequate,
in scope and quality, as a thesis for the degree of Master of Science.

Prof. Dr. Bahattin KANBER

Supervisor

Examining Committee Members: Signature

Prof. Dr. İbrahim H. GÜZELBEY   ....

Prof. Dr. Bahattin KANBER   ....

Assoc. Prof. Dr. Ahmet ERKLİĞ   ....

Assist. Prof. Dr. Ö. Yavuz BOZKURT   ....

Assist. Prof. Dr. Eyüp YETER   ....

I hereby declare that all information in this document has been obtained and presented in accordance with academic rules and ethical conduct. I also declare that, as required by these rules and conduct, I have cited and referenced all material and results that are not original to this work.

Nurettin Furkan DOĞAN

ABSTRACT

ELASTO-PLASTIC ANALYSIS OF THICK BEAMS USING MESHFREE METHODS

DOĞAN, Nurettin Furkan

M.Sc. in Mechanical Engineering

Supervisor: Prof. Dr. Bahattin KANBER

July 2015, 57 pages

In this thesis, elasto-plastic analysis of thick beams is presented using Point Interpolation Method (PIM) and Radial Point Interpolation Method (RPIM) using two different integration schemes. In the first one, standard Gauss integration scheme is used using background integration cells. In the second one, however, a nodal integration scheme is used based on Taylor Series. A computer program is developed for these algorithms in MATLAB. Different case studies are solved using developed program and they are tested for various support domain sizes and RPIM shape parameters. Their effects are investigated on the solution accuracy in details.

ÖZET

AĞSIZ YÖNTEMLER KULLANILARAK ELASTO-PLASTİK KALIN KİRİŞLERİN ANALİZİ

DOĞAN, Nurettin Furkan

Yüksek Lisans Tezi, Makine Mühendisliği Bölümü

Tez Yöneticisi: Prof.Dr. Bahattin KANBER

Temmuz 2015, 57 sayfa

Bu tezde, kalın kirişlerin elasto-plastik analizi Noktasal İnterpolasyon Yöntemi (NİY) ve Radyal Noktasal İnterpolasyon Yöntemi (RNİY) ile iki farklı integrasyon yöntemi kullanılarak gerçekleştirilmiştir. Birincisi integrasyon hücrelerinin kullanıldığı Gauss integrasyon yöntemi, ikincisi ise Taylor serisinin kullanıldığı noktasal integrasyon yöntemidir. Geliştirilen program kullanılarak MATLAB programı üzerinde kaynak kodları hazırlanmıştır. Farklı örnekler hazırlanan kaynak kodları ile çözülmüş. Farklı destek alanı büyüklükleri ve RNİY şekil parametrelerinin çözümler üzerine etkileri incelenmiştir.

Anahtar Kelimeler: Ağsız yöntemler, NİY, RNİY, elasto-plastik, kalın kirişler

To my wife and my unborn baby . . .

ACKNOWLEDGEMENTS

I would like to express the deepest appreciation to my supervisor Prof. Dr. Bahattin KANBER for his guidance, suggestions and encouragement during my master education and preparation of this thesis.

And also, I would like to thank to my parents, my siblings and my friends for the unwavering moral and emotional support.

CONTENT

LIST OF TABLES

LIST OF FIGURES

LIST OF SYMBOLS

x_Q = Point of interest

$u(x)$ = Field function

$B(x)$ = Basis function

a = Coefficient for basis function

$\boldsymbol{a}$ = Coefficient vector of basis function

p = Polynomial basis function

$\boldsymbol{p}$ = Vector of polynomial basis function

$\boldsymbol{P}_Q$ = Moment matrix of polynomial basis function

$\boldsymbol{u}^{sd}$ = Generalized displacement matrix

$\boldsymbol{\phi}$ = Shape function matrix

R = Radial basis function

$\boldsymbol{R}$ = Vector of radial basis function

α_c = Dimensionless shape parameter of RPIM

q = Dimensionless shape parameter of RPIM

$\boldsymbol{R}_Q$ = Moment matrix of radial basis function

$\boldsymbol{\varepsilon}$ = Total strain vector

$\boldsymbol{\varepsilon}^e$ = Elastic strain vector

$\boldsymbol{\varepsilon}^p$	=	Plastic strain vector
$\boldsymbol{\sigma}$	=	Stress vector
$\boldsymbol{E}$	=	Material property matrix (constitutive matrix)
$\bar{u}$	=	Axial displacement
θ	=	Rotation of normal, slope
β	=	Rotation due to transverse shear deformation
$\boldsymbol{\varepsilon}_f$	=	Flexural strain vector
$\boldsymbol{\varepsilon}_s$	=	Shear strain vector
$\boldsymbol{B}_f$	=	Curvature- displacement matrix
$\boldsymbol{B}_s$	=	Shear strain- displacement matrix
$\boldsymbol{\varphi}$	=	Basic unknown vector
$\boldsymbol{K}_f$	=	Local flexural stiffness matrix
$\boldsymbol{K}_s$	=	Local shear stiffness matrix
$\boldsymbol{f}$	=	Applied force vector
H'	=	Hardening parameter
$q1, q2$	=	Gaussian quadrature points
$w1, w2$	=	Gaussian weights
Jac	=	Jacobian
sd	=	Support domain size

CHAPTER 1

INTRODUCTION

1.1. General Introduction

In engineering design, numerical methods have a crucial role and due to the requirement in simulate and optimizing engineering systems brace this crucial role. Meshfree methods are distinctive part of the numerical methods that show a great improvement in the last decade. They are arisen from the lack of the other numerical methods such as finite element method (FEM), finite difference method (FDM), finite volume method (FVM) and boundary element method (BEM).

These numerical methods are mostly works very well. However, they have some disadvantages [1]:

- In FEM, BEM and FDM, predefined meshes (elements, grids, volumes) are required. And these meshes must be well-posed even problem is so complicated. This requirement causes excessive computation time, hence excessive cost.

-In large deformation problems, solution accuracy can be decreased, even process can break down due to element distortions.

-In FEM, elements are considered as indivisible. So, in some problems as breakage of material case it is very difficult to success a good model simulation. Due to this difficulty, problems can be mispresented and serious solution errors can be seen.

-In crack growth problems, the simulation can be very difficult especially with complex growth path due to discontinuities.

-In FEM, model is usually over stiff. In this case, some problems like locking can be occurred. And as a result, solution accuracy decreases, also extremely high stresses can be seen on region such as crack tips or contact faces.

-To handle these problems, re-meshing is applied. But, this application needs complex algorithms and an extra computation time.

All these problems above, lead to find a new numerical approach: Meshfree methods. With these methods, predefined mesh requirement has been eliminated, thus the problems above have been solved on a large scale. In meshfree methods, instead of using predefined meshes, the problem domain is represented with more flexible way: arbitrary distributed nodes. These methods introduce great conveniences. Nodes can be added or deleted freely in order to get desired accuracy.

1.2. Layout of Thesis

A literature review of the some Meshfree methods is presented in Chapter two. The basic properties of Point Interpolation Methods and their shape function construction are presented in Chapter three. In next chapter, Chapter four, elasto-plastic beam theories are presented and detailed formulation of thick beams are given. In Chapter five, PIM and radial PIM (RPIM) implementation for thick beam are presented. Later, in Chapter six, some benchmark problems' solutions are presented. Finally, in Chapter seven, the conclusions are introduced.

CHAPTER 2

LITERATURE SURVEY

2.1. Introduction

In FEM, FDM and FVM, the problem domain is discretized into meshes. And a mesh is defined as any of the open spaces or interstices between the strands of a net that is formed by connecting nodes in a predefined manner [1, 2]. Mesh is used as grids in FDM, volume in FVM and element in FEM. In all methods, mesh must be predefined to ensure a relationship between nodes.

Meshfree methods are used to create system algebraic equations for the whole problem domain without using any predefined mesh for domain discretization. In the meshfree methods, a set of nodes distributed within the problem domain and on the boundaries are used to represent the problem domain and also its boundaries. Then, the field functions are approximated locally using these nodes and there is no need an element or connectivity of the nodes for approximation. There are number of meshfree methods can be found in the literature. The EFG (Element Free Galerkin) Method, the SPH (Smoothed Particle Hydrodynamics) Method, the MLPG (Meshless Local Petrov-Galerkin) Method, the PIM (Point Interpolation Method) and the RPIM (Radial Point Interpolation Method) are some of these methods.

The EFG, SPH and MLPG methods will be represented shortly in this section. Also, detailed review of PIM and RPIM methods are given in Section 2.2 which are used in this study.

2.2. Overview of Meshfree Methods

2.2.1. Point Interpolation Method

The Point Interpolation Method (PIM) is a meshfree method, proposed by Liu and Gu [3, 4]. This method came out as a solution of some problems in Moving Least Square (MLS) based meshfree methods. One of these problems is the complex structure of

algorithms in computation of shape functions and the other one is difficulties in implementation of the essential boundary conditions. These problems cause increases in computation time with the result that increase in computational cost. Some different solution paths are proposed for these problems [5- 8].

In PIM, the field variable at a point is interpolated by the variables in the influence domain of this point. In this method, interpolation shape functions are constructed using polynomials which are selected from Pascal's triangle. These functions are suitable for Kronecker delta function property very well. Not like other meshfree methods, it is easy to construct interpolation shape functions due to polynomial base and easy to apply the essential boundary conditions due to Kronecker delta function property.

However, PIM has some problems. The main problem is the possibility of a singular moment matrix. A couple of reasons may cause this problem: improper distributed nodes in local domain and improper monomial selection in basis function [1, 4, and 5].

To eliminate singularity in moment matrix, several strategies have been proposed [1, 4, 5, and 10]. One of these strategies is to move the nodes in support domain with a small amount randomly [1, 4]. Also, rotational coordinate transformation is proposed [1, 13]. These solutions work on disappearing improper distributed node effect. However, in these two strategies there is still a chance to obtain singular moment matrix.

The matrix triangularization algorithm (MTA) is also proposed by Liu and Gu [9] to overcome singular moment matrix problem of polynomial PIM. Also, this algorithm works well to avoid singularity in moment matrix. However, the MTA may be numerically unstable in some cases [9].

A diagonal offset algorithm is another strategy which is proposed by Kanber and Bozkurt [11]. This algorithm works very well to avoid singularity issue and gives accurate results.

Another strategy to eliminate singular moment matrix is the use of radial basis functions (RBFs) to construct PIM shape functions which is proposed by Wang and Liu [10, 14].

PIMs can be formulated by the combination of Galerkin weak form [3], the local Petrov-Galerkin weak form [12], the boundary integration equation (BIE) [15, 16].

The PIMs have a large application area due to its high accuracy, easiness to shape function construction and implementation of boundary conditions.

2.2.2. Radial Point Interpolation Method

The radial point interpolation method (RPIM) is proposed by Wang and Liu [10]. In RPIM, radial basis functions are used instead of polynomial basis function. Using radial basis functions with proper shape parameters works perfectly. Radial basis PIM (RPIM) has also Kronecker delta function property. However, this method requires more nodes to obtain accurate results as PIM [2].

It is very important issue to use proper shape parameter in radial basis functions to construct PIM shape function. Because, shape parameters affect the accuracy and performance of RPIM. The effect of shape parameters were studied deeply in [10, 14, 17, and 18] and optimum shape parameters were proposed in these studies. For RPIM shape parameter q, values between 1.0 and 3.0 is recommended for 3D problems. 1.03 is the best choice of q for both 3D and 2D problems. For RPIM shape parameter α_c, better results can be obtained when it is used as 3.0 and 4.0 [14].

2.2.3. Smoothed Particle Hydrodynamics

Smoothed particle hydrodynamics (SPH) method is initially used to understand some astrophysical problems in three-dimension [19]. A set of moving particles which does not have any predefined background cells are used to represent physical problem domain. The mathematical model of physical problem is constructed using partial differential equations which are transformed into selected finite integral form to compute over the integral form. Most applications of SPH are related with astrophysical problems and fluid dynamics such as star formation, stellar collisions, meteor impacts [20] and elastic flow [21], incompressible flows [22]. Also, SPH is adapted to impact problems [23- 27], fracture simulation [28, 29], elasto-plastic case

such as metal forming [30, 31], simulation of explosive welding [32] and brittle solids [33]. Additionally, SPH has been applied to explosion and penetration simulations [34-37]. Smoothed particle hydrodynamics (SPH) method still has some problems such as stability and consistency, especially in solid mechanic applications.

2.2.4. Element Free Galerkin Method

Element-free Galerkin (EFG) method is proposed by Belytschko et al. [38] based on the diffuse elements method (DEM). In EFG method, the problem domain and boundaries are represented by arbitrary distributed nodes and shape function construction is utilized by using moving least squares (MLS) approximation on these nodes. So, EFG does not need any mesh generation. On the other hand, a set of background cells are required to perform Galerkin weak form integration.

In literature, there are very large application areas of EFG method like solid mechanics, fluid mechanics, electromagnetic field and heat transfer problems. In solid mechanics, many different elastic and plastic applications can be found such as beam [39], shell [40], plate [41], plane stress [42] and plane strain [43] problems.

2.2.5. Meshless Local Petrov-Galerkin Method

Meshless Local Petrov Galerkin (MLPG) method is proposed by Atluri and Zhu [44], later is developed by Atluri and Shen [50]. This method is accepted as a truly meshfree method due to any requirement of background cell for interpolation or integration process despite of the other methods. The MLPG method is based on a weak form which is constructed on a local subdomain. The method only needs nodal information and element connectivity does not required. Thus, this leads a really simple pre-processing.

Because of the simplicity of the method, wide range of applications can be found in the literature such as large deformation problems [45], fracture mechanics [46], beam problems [47], plate problems [48], shell problems [2] and fluid mechanics problems [49].

2.3. Conclusion on Literature Survey

Literature survey shows that both PIM and RPIM have some points that directly affect the solution accuracy. As a summary, they can be given as:

a) Support domain size,
b) Radial basis function shape parameters and
c) Integration scheme.

And also literature review shows that elasto-plastic analysis of thick beams has not been carried out using PIM and RPIM. Investigating of solution performances of PIM and RPIM on the elasto-plastic analysis of thick beams is the main concern of this thesis.

CHAPTER 3

POINT INTERPOLATION METHODS

3.1. Introduction

Point interpolation method (PIM) is a simple and useful meshfree method that is originally proposed by [3, 4]. In point interpolation method, field variables are approximated by letting the interpolation function on each distributed node. In PIM, the shape functions have Kronecker delta function property. Due to this property, the application of essential and natural boundary conditions is very simple and there is no need to an extra algorithm for this purpose [1]. Polynomial and radial basis functions are used to obtain PIM shape functions in literature. In Section 3.4, shape function construction procedure will be explained in detail.

3.2. A Brief Review on Solution Procedure for Meshfree Methods

Solution procedure can be summarized as domain discretization, field variable interpolation, formation of system equations and solution the meshfree equations. In domain discretization, the set of scattered nodes are used to represent the problem domain. Then, boundary conditions and loading conditions are defined. Here, the number of the nodes depends on the requirement in the accuracy of modelling and solution. After problem domain representation, the shape functions are constructed for each node in the local domain. As a third step, the system equations are formatted. The equations of a meshfree method can be formulated by a strong form system equation or weak form system equation. All these functions constructed as nodal form, so there is an assembling procedure needed to obtain a global system equations and different assembling procedures are used for different meshfree method. At the last step, global system equations are solved by using different solving method. In static problems, field variables (displacement) at all nodes are obtained firstly. Then, stress and strain can be calculated using constitutive equations and strain- displacement relations.

3.3. Basic Definitions on Meshfree Methods

In meshfree methods, the most encountered terms can be listed as local domain and background cells. These two terms are briefly explained in the following sections.

3.3.1. Local Domains

In FEM, predefined elements are used to approximate the field variables. And the shape function construction is done before using elements which the number of node in the element is predefined. Also, elements are used for integration purpose. As mentioned before, in meshfree methods, the shape functions are constructed on the nodes in the local domain. Also, local domain construction in meshfree methods does not contain any predefined node information.

Local domain is categorized in two different terms; support and influence domain. Support domain term is used to define the area where the interpolation of a point of interest is done. Also, it is used to define the number of nodes which include in the shape function construction. Influence domain is used to define the area that a node exerts an influence upon. Influence domains can be different from node to node and represents the influence of the node [1].

3.3.2. Background Cells

In meshfree methods based on Galerkin weak form, the problem domain is discretized to non-overlapping background cells to perform the integration of global system equations.
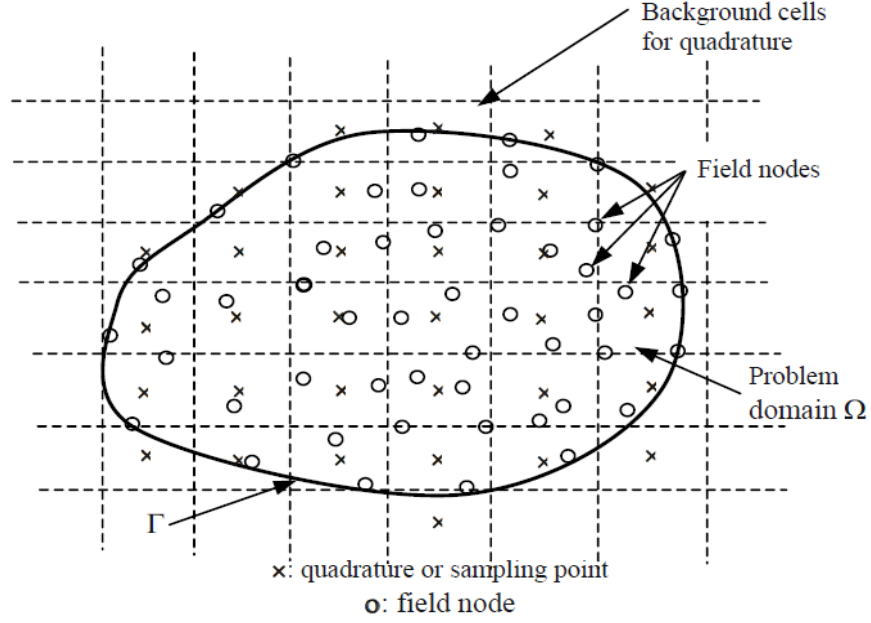
Figure 3. 1. Local domains and background Cells in Problem Domain Ω [1]

3.4. Point Interpolation Method Shape Functions

Shape function construction is the most important issue in meshfree methods. As mentioned before, shape function construction in meshfree methods is performed on a node by using small number of local support node vicinity of the point of interest and it is special for the node. Consider a field function $u(\mathbf{x})$ defined in the problem domain Ω that represented by a regularly distributed nodes. The field function $u(\mathbf{x})$ can be approximated on the point of interest x_Q as:

$$u(x, x_Q) = \sum_{i=1}^{n} B_i(x)a_i \tag{3.1}$$

where $B_i(x)$ is the basis function defined in the Cartesian coordinate, a_i is the unknown coefficient for the basis function, n is the number of nodes in a local support domain.

Point interpolation method (PIM) is divided into two parts upon basis function type. First polynomial PIM is developed by Liu and Gu [3, 4] and second type is the Radial Point Interpolation Method (RPIM) which is developed by Wang and Liu [10].

3.4.1. Polynomial Point Interpolation Method Shape Functions

In polynomial PIM, as the name suggests the polynomial basis function is used. Hence, the Equation 3.1 becomes:

$$u(x, x_Q) = \sum_{i=1}^{n} p_i(x)a_i = \boldsymbol{p}^T(x)\,\boldsymbol{a}(x_Q) \tag{3.2}$$

where p_i is the basis function of monomials, $\boldsymbol{a}$ is the unknown coefficient vector of monomial.

The polynomial $p_i(x)$ is constructed using Pascal triangles. And $p_i(x)$ in one dimension is:

$$\boldsymbol{p}^T(x) = [1, x, x^2, x^3, x^4, \ldots, x^{n-1}] \tag{3.3}$$

The unknown coefficient vector $\boldsymbol{a}_i$ in Equation 3.2 can be obtained by solving Equation 3.2 at the n support nodes. At point of interest node i, we have nodal value of $u(x_i)$:

$$u(x_i) = \boldsymbol{p}^T(x_i)\boldsymbol{a} \tag{3.4}$$

The generalized displacement vector u^{sd} can be written in matrix form as:

$$\boldsymbol{u}^{sd} = \boldsymbol{P}_Q\boldsymbol{a} \tag{3.5}$$

where $\boldsymbol{u}^{sd} = \{[w_1,\ \theta_1, w_2,\ \theta_2, \ldots, w_n, \theta_n]^T\}$ and moment matrix $\boldsymbol{P}_Q$ of local domain for 1D case is:

$$\boldsymbol{P}_Q = \begin{bmatrix} 1 & x_1 & \ldots & x_1^{n-1} \\ 1 & x_2 & \ldots & x_2^{n-1} \\ \vdots & \vdots & \ddots & \vdots \\ 1 & x_n & \ldots & x_n^{n-1} \end{bmatrix} \tag{3.6}$$

where n is the number of node in the support domain. If the inverse of moment matrix exists, unknown coefficient vector $\boldsymbol{a}$:

$$\boldsymbol{a} = \boldsymbol{P}_Q^{-1}\boldsymbol{u}^{sd} \tag{3.7}$$

Finally, substituting Equation 3.7 into the Equation 3.2 gives:

$$u(x, x_Q) = \sum_{i=1}^{n} p_i(x)a_i(x_Q) = \boldsymbol{\phi}(x)\boldsymbol{u}^{sd} \tag{3.8}$$

11

where the matrix of the PIM shape function $\boldsymbol{\phi}(x)$ is:

$$\phi = \boldsymbol{p}^T(x)\boldsymbol{P}_Q^{-1} = [\phi_1(x) \quad \phi_2(x) \dots \quad \phi_n(x)] \tag{3.9}$$

3.4.2. Radial Point Interpolation Method Shape Functions

In Radial Point Interpolation Method (RPIM), radial functions are used as a basis function. Thus, Equation 3.1 becomes:

$$u(x, x_Q) = \sum_{i=1}^{n} R_i(x)a_i(x_Q) = \boldsymbol{R}^T(x)\boldsymbol{a} \tag{3.10}$$

where $\boldsymbol{a}$ is the unknown coefficient vector for the radial basis function (RBF), n is the number of nodes in support domain and $R_i(x)$ is the basis function with the distance r between point of interest x_Q and x_i which for 1D problem is $r = x_Q - x_i$.

While the radial basis function vector $\boldsymbol{R}$ is used itself without powers in the original RPIM [1, 2], it can be used in the following form to increase its accuracy:

$$\boldsymbol{R}^T = [R_1(r_1)^0, R_2(r_2)^1, R_3(r_3)^2, \dots, R_n(r_n)^{n-1}] \tag{3.11}$$

The different types of radial basis functions exist in literature, the typical radial basis functions are listed below:

Table 3. 1. Typical RBFs in Literature

	Name	Expression	Shape Parameters
1	Multi-quadrics	$R_i(x, y) = (r_i^2 + \alpha_c d_c)^q$	α_c, q
2	Logaritmic RBF	$R_i(r_i) = r_i^\eta \log r_i$	η
3	Gaussian (exp)	$R_i(x, y) = \exp(-cr_i^2)$	c
4	Thin Plate Spline(TPS)	$R_i(x, y) = r_i^\eta$	η

In this thesis, multi-quadrics radial function is used as a basis function and the shape parameters which are proposed in [10] are used to examine the effect on the solution convergency.

The unknown coefficient vector $\boldsymbol{a}_i$ can be obtained by enforcement of Equation 3.10 for all the n support nodes. At point of interest node i, we have nodal value of $u(x_i)$:

$$u(x_i) = \boldsymbol{R}^T(x_i)\boldsymbol{a} \tag{3.12}$$

12

And again, the generalized displacement vector, u^{sd} can be written in the form:

$$u^{sd} = R_Q a \qquad (3.13)$$

R_Q is the moment matrix of RBFs and can be written as follows:

$$R_Q = \begin{bmatrix} R_1(r_1)^0 & R_2(r_1)^1 & \dots & R_n(r_1)^{n-1} \\ R_1(r_2)^0 & R_2(r_2)^1 & \dots & R_n(r_2)^{n-1} \\ \vdots & \vdots & \ddots & \vdots \\ R_1(r_n)^0 & R_2(r_n)^1 & \dots & R_n(r_n)^{n-1} \end{bmatrix} \qquad (3.14)$$

If the R_Q matrix is invertible vector of coefficients a is:

$$a = R_Q^{-1} u^{sd} \qquad (3.15)$$

As a result, substituting Equation 3.15 into Equation 3.10 gives:

$$u(x, x_Q) = \sum_{i=1}^{n} R_i(x) a_i(x_Q) = \boldsymbol{\phi}(x) u^{sd} \qquad (3.16)$$

where the matrix of the RPIM shape function $\boldsymbol{\phi}(x)$ is:

$$\boldsymbol{\phi}(x) = R^T(x) R_Q^{-1} = [\phi_1(x) \quad \phi_2(x) \dots \quad \phi_n(x)] \qquad (3.17)$$

CHAPTER 4

ELASTO-PLASTIC BEAM THEORIES

4.1. Introduction

In engineering, the prediction of failure holds a very important place due to the safety of design. Beams are mechanical components that are widely used in engineering design. Several beam theories have been proposed so far based on different assumptions. In this chapter, the basic essentials of elasto-plastic analysis and the most widely used beam theories: Euler-Bernoulli and Timoshenko Beam Theories will be introduced.

4.2. The Fundamentals of Elasto-Plastic Analysis

The theory of plasticity undertakes the complementary role of the theory of elasticity and deals with the stress-strain relation of structure in plastic region as well as in elastic region.

After yielding point (i.e. in plastic region), strain increments can be separated into elastic and plastic components as [51, 52, 53]:

$$d\boldsymbol{\varepsilon} = d\boldsymbol{\varepsilon}^e + d\boldsymbol{\varepsilon}^p \tag{4.1}$$

where e denotes elastic and p denotes plastic components. Since, in plastic region, Hooke's law is no longer enough to provide a relationship between the incremental stress and elastic strain, this relation for plastic material is covered for the current state and the incremental changes of stress and strain for different plasticity assumptions like elastic-perfectly plastic materials, elastic-work hardening materials, etc. Stress-strain relation in elasto-plastic case can be written in general form as:

$$d\boldsymbol{\sigma} = \boldsymbol{E}d\boldsymbol{\varepsilon}^e \quad \text{or} \quad d\boldsymbol{\sigma} = \boldsymbol{E}(d\boldsymbol{\varepsilon} - d\boldsymbol{\varepsilon}^p) \tag{4.2}$$

where $\boldsymbol{E}$ is the material property matrix.

Elasto-plastic analysis have three essential components which are a yield criterion, a flow rule and a hardening rule. Yield criterion deals with the states of stress is beyond the yielding. In the literature, there are different criterions available. In all criterions, transition from elastic to plastic region is defined by using different aspects. In von Misses criteria, yielding occurs when the elastic distortion energy reaches a critical value which is the maximum value of elastic distortion energy. In this study, von Misses yield criteria is used. On the other hand, in Tresca yield criteria, yielding occurs when the maximum shear stress reaches a certain value.
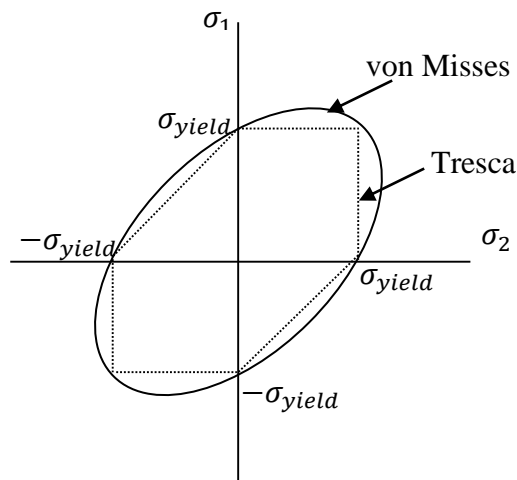
Figure 4. 1. Yield Criterions Representation

Another essential of the plasticity is the flow rule. The flow rule defines a relationship between stress increment and strain increment after yielding. The last component of plasticity is hardening rule, and it describes how the yield criterion is modified by straining beyond the initial yield. The hardening rule can be presented as isotropic hardening or kinematic hardening [53, 54]. In isotropic hardening, the yield surface can expand without any transition under loading. i.e. when the stress state reaches beyond the initial yield point, it has a new yield point in loading and after unloading in compressive loading situation the yield point will have a greater value. However, in kinematic hardening, the yield surface moves as a rigid body in loading. i.e. when the stress state reaches beyond the initial yield point, it has a new yield point in loading and in compressive loading situation the yield point will have a smaller value from the initial yield point. Following figures will be easier way to explain these two rules.
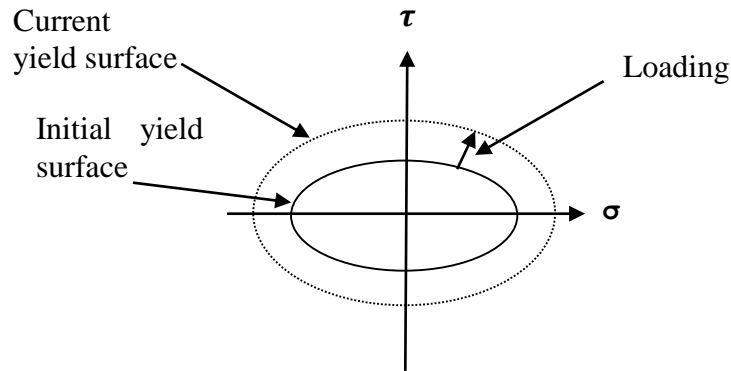
Figure 4. 2. Isotropic Hardening Model Representation
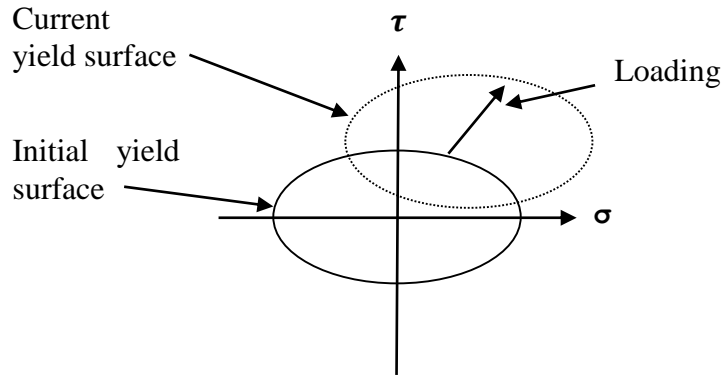
Figure 4. 3. Kinematic Hardening Model Representation

4.3. Beam Theories

In this section, beam theories will be summarized shortly. The two important beam theories are:

- Euler- Bernoulli beam theory
- Timoshenko beam theory

4.3.1. Euler- Bernoulli Beam Theory

The Euler- Bernoulli beam theory is proposed in 18th century by Leonard Euler and Daniel Bernoulli. In Euler- Bernoulli beam theory, the shear effect on deformation is neglected, so this theory is mostly useful for thin beams. There are some assumptions in this theory [52]:

a. Cross-sectional area remains plane after deformation.
b. The normal line to the cross-sectional area remain straight after deformation.

c. The normal to the cross-sectional plane must be remain normal after deformation.

4.3.2. Timoshenko Beam Theory

The Timoshenko beam theory is proposed by Stephen Timoshenko in 1921 [55]. As mentioned before, in Euler- Bernoulli beam theory the shear effect on the deformation does not considered. However, the shear deformation takes a place in real problems. In Timoshenko beam theory, the shear effect is considered in solutions. This causes more effective solutions and makes Timoshenko beam theory perfect for thick beam problems. In this study, Timoshenko beam theory is used to elasto- plastic analysis. In this theory, there are three assumptions existed as Euler- Bernoulli beam theory:

a. Cross-sectional area remains plane after deformation.
b. The normal line to the cross-sectional area remain straight after deformation.
c. The normal to the cross-sectional plane cannot be remain normal after deformation.

There are two approaches to the elasto-plastic analysis of Timoshenko beams [51]:

a. Non-layered approach: In this study, non-layered approach is used to figure out plasticity in the cross-section. This approach states that when the bending moment reaches the yield moment, the whole cross-section becomes plastic instantaneously. However, in reality there is always a gradual plastification in the beam and plastic are spreads inwards from the outer fibres.
b. Layered approach: In this approach, the cross-section is divided into layers. And, spread of plasticity is observed by using these layers. Of course, that is reasonable the increasing in number of layers causes more realistic solutions.

In a Timoshenko beam (Figure 4.4), as we said before, it is assumed that normal to the neutral axis before deformation remain straight but cannot be remained normal to the neutral axis after deformation. This means that axial displacement $\bar{u}$ at any point (x, z) can be expressed in terms of $\theta(x)$ rotation of the normal. So, displacement field is [51, 52, 56]:

$$\bar{u}(x,z) = -z\theta(x)$$

$$\bar{w}(x,z) = w(x)$$

(4.3)

17

where $\theta(x)$ rotation of the normal is equal to:

$$\theta(x) = \frac{d\bar{w}}{dx} - \beta \tag{4.4}$$

$\frac{dw}{dx}$ denotes the slope of the neutral axis and β denotes a rotation due to transverse shear deformation.
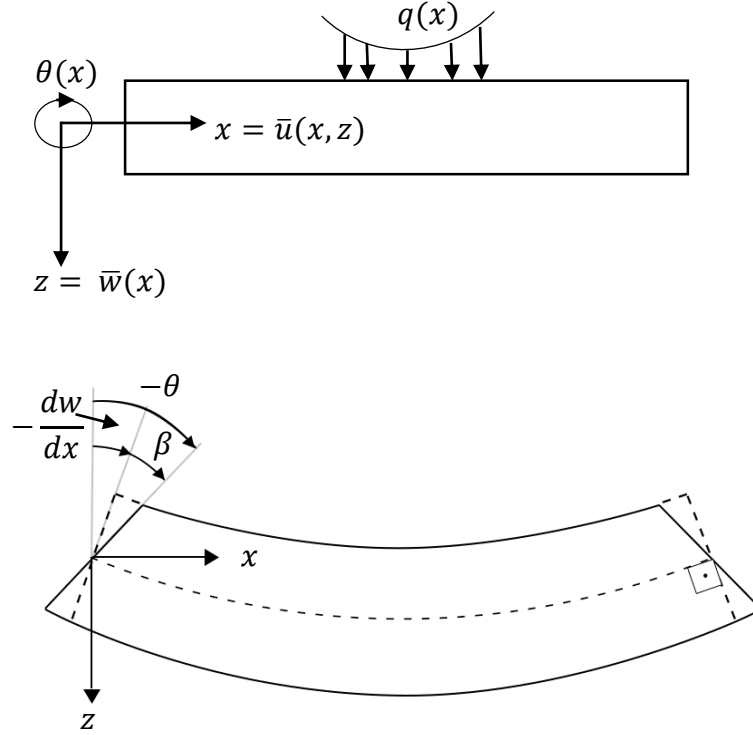
Figure 4. 4. Timoshenko beam

In Timoshenko beam, the constitutive relations are given by:

$$\left.\begin{array}{c} \sigma_x = E\varepsilon_x \\[2mm] \tau_{xz} = kG\gamma_{xz} \end{array}\right\} \tag{4.5}$$

where axial strain ε_x is:

$$\varepsilon_x = \frac{\partial \bar{u}}{\partial x} = -z\frac{d\theta}{dx} \tag{4.6}$$

and shear strain γ_{xz} is:

$$\gamma_{xz} = \beta = \frac{\partial \bar{u}}{\partial x} + \frac{\partial \bar{w}}{\partial x} = -\theta + \frac{dw}{dx} \tag{4.7}$$

18
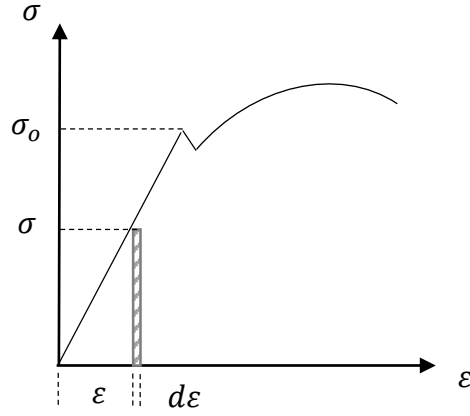
Figure 4. 5. Stress- strain diagram

For linear, elastic and isotropic material, area under the stress-strain curve in Figure 4.5 is the internal energy. Thus:

$$\int d\mathrm{u} = \int_0^\varepsilon \frac{1}{2}\sigma\, d\varepsilon \quad \rightarrow \quad \mathrm{u} = \frac{1}{2}\sigma\,\varepsilon \tag{4.8}$$

where u is the internal energy density.

In Timoshenko beam theory, the internal energy considers both bending and shear contributions:

$$U = \int u\, dV = \frac{1}{2}\int_V \sigma\varepsilon_x dV + \frac{1}{2}\int_V \tau_{xz}\gamma_{xz} dV \tag{4.9}$$

Using Equation 4.5 and $dV = dAdx$, we obtain the total internal energy in terms of generalized displacements:

$$U = \frac{1}{2}\int_V E\varepsilon_x{}^2 dV + \frac{1}{2}\int_V kG\gamma_{xz}{}^2 dV$$

$$= \frac{1}{2}\int_{-a}^a EI_z \left(\frac{\partial\theta_z}{\partial x}\right)^2 dx + \frac{1}{2}\int_{-a}^a kG \left(\frac{\partial w}{\partial x} - \theta_z\right)^2 dx \tag{4.10}$$

19

CHAPTER 5

PIM AND RPIM FORMULATION FOR THICK BEAMS

5.1. Basic Equations for Thick Beams

In a local support domain, the nodal lateral displacement w_i and slope θ_i in a local node can be defined in terms of shape functions as follows:

$$\left.\begin{aligned} w_i &= \phi_1 w_1 + \phi_2 w_2 + \cdots + \phi_n w_n \\ \theta_i &= \phi_1 \theta_1 + \phi_2 \theta_2 + \cdots + \phi_n \theta_n \end{aligned}\right\} \tag{5.1}$$

In Timoshenko beam theory, shear effect on the displacement is considered as mentioned before. Thus we have a couple of relationship as; the curvature-displacement and shear strain-displacement relationship in local support domain. The curvature- displacement relationship is:

$$\epsilon_f = -\frac{d\theta}{dx} = \boldsymbol{B}_f \boldsymbol{\varphi} \tag{5.2}$$

And shear strain- displacement relationship in local support domain is:

$$\epsilon_S = \frac{dw}{dx} - \theta = \boldsymbol{B}_S \boldsymbol{\varphi} \tag{5.3}$$

where $\boldsymbol{\varphi}$ is the basic unknowns, nodal vector of displacements in our case , $\boldsymbol{B}_f$ is the curvature-displacement matrix:

$$\boldsymbol{B}_f = \begin{bmatrix} 0 & \frac{d\phi_1}{dx} & 0 & \frac{d\phi_2}{dx} & \dots & 0 & \frac{d\phi_n}{dx} \end{bmatrix} \tag{5.4}$$

and $\boldsymbol{B}_s$ is the shear strain-displacement matrix:

$$\boldsymbol{B}_s = \begin{bmatrix} \frac{d\phi_1}{dx} & -\phi_1 & \frac{d\phi_2}{dx} & -\phi_2 & \dots & \frac{d\phi_n}{dx} & -\phi_n \end{bmatrix} \tag{5.5}$$

Using strain-displacement relationships and the total energy expression in Equation 4.10 which are proposed by [51, 57], the governing equation can be expressed as:

$$[\boldsymbol{K}_f + \boldsymbol{K}_s]\boldsymbol{\varphi} - \boldsymbol{f} = 0 \tag{5.6}$$

where $\boldsymbol{K}_f$ and $\boldsymbol{K}_s$ are local stiffness matrices , $\boldsymbol{f}$ is the applied load vector which are expressed as:

$$\left.\begin{array}{c} \boldsymbol{K}_f = \int_{x1}^{x2}[\boldsymbol{B}_f]^T(EI)\boldsymbol{B}_f dx \\[2mm] \boldsymbol{K}_s = \int_{x_1}^{x_2}[\boldsymbol{B}_s]^T(GA)\boldsymbol{B}_s dx \\[2mm] \boldsymbol{f} = \int_{x_1}^{x_2}[\phi_1 \quad 0 \quad \phi_2 \quad 0]^T q\, dx \end{array}\right\} \tag{5.7}$$

where EI is the *flexural rigidity* and GA is the *shear rigidity*, ϕ is the nodal shape function which can be constructed either using PIM or RPIM methods.

Bending moments and shear forces on each support domain can be expressed as [51]:

$$M = (EI)\boldsymbol{B}_f\boldsymbol{\varphi} = \left(\frac{EI}{l}\right)(\theta_1 - \theta_2) \tag{5.8}$$

where θ_1 and θ_2 are slopes on the local nodes, l is integration domain length.

Shear force varies linearly over support domain, if we evaluate it on the mid-point of domain and assume that it is constant over the domain:

$$Q = (GA)\boldsymbol{B}_s\boldsymbol{\varphi} = (GA)\left\{\left(\frac{w_2 - w_1}{l}\right) - \left(\frac{\theta_1 + \theta_2}{2}\right)\right\} \tag{5.9}$$

The value of the ultimate moment, in plastic condition can be expressed in terms of yield stress σ_0 as:

$$M_0 = \int_{b(-t/2)}^{b(t/2)} \int_{-t/2}^{t/2} z\, \sigma_0 dz\, dy \tag{5.10}$$

where $M_0 = \sigma_0(bt^2/4)$ for a rectangular beam.

After yielding flexural rigidity EI becomes elasto-plastic flexural rigidity:

$$(EI)_{ep} = EI\left(1 - \frac{EI}{EI + H'}\right) \tag{5.11}$$

21

where strain hardening $H^{'}$ parameter is defined as:

$$H^{'} = \frac{dM}{(d\epsilon_f)_p} \qquad (5.12)$$

5.2. Integration Schemes

As mentioned above, using virtual work approach the governing equation for the Timoshenko beam is given in Equation 5.6 as $[K_f + K_s]\boldsymbol{\varphi} - \boldsymbol{f} = 0$ where $\boldsymbol{K}_f$ and $\boldsymbol{K}_s$ were flexural and shear local stiffness matrices respectively, $\boldsymbol{f}$ was the applied force vector. To evaluate Equation 5.7, two different integration schemes are used:

5.2.1. Gauss Integration Method

First one is standard Gauss integration. In this method, quadrature cells (background cells) are used to integration. And, the shape functions are calculated for each node in the support domain. Two point Gauss integration is used to calculate flexural nodal stiffness matrix and one point Gauss integration is used for shear nodal stiffness matrix calculation due to shear locking phenomenon. In two-point Gauss integration, the integral is approximated as [58]:

$$I = \int_a^b f(x)dx \approx w_1 f(q_1) + w_2 f(q_2) \qquad (5.13)$$

Thus, local stiffness matrices are:

$$\boldsymbol{K}_f = EI * (Jac) * \left[(w_1)\left([\boldsymbol{B}_f]^T_{\mathbf{q1}} * [\boldsymbol{B}_f]_{\mathbf{q1}}\right) + (w_2)\left([\boldsymbol{B}_f]^T_{\mathbf{q2}} * [\boldsymbol{B}_f]_{q2}\right) \right]$$

$$\boldsymbol{K}_s = GA * (Jac) * \left[(w)\left([\boldsymbol{B}_s]^T_{\mathbf{q}} * [\boldsymbol{B}_s]_{\mathbf{q}}\right) \right] \qquad (5.14)$$

where *Jac* is the Jacobian, w,w_1,w_2 are weights, q,q1,q2 are quadrature points which can be seen in Table 5.1 and $\boldsymbol{B}_f$ and $\boldsymbol{B}_s$ are presented in Equation 5.4 and 5.5 respectively.

Table 5. 1. Weights and quadrature points used in Gauss Integration Formulas

Points	Weighting Factors	Function Arguments
1	$w=2$	$q=0$
2	$w_1 = 1.000000000$ $w_2 = 1.000000000$	$q_1 = -0.577350269$ $q_2 = 0.577350269$
3	$w_1 = 0.555555556$ $w_2 = 0.888888889$ $w_3 = 0.555555556$	$q_1 = -0.774596669$ $q_2 = 0.000000000$ $q_3 = 0.774596669$

5.2.2. Nodal Integration Method

The second integration scheme is the nodal integration proposed by Liu et al [59]. In this method, integration function (nodal stiffness matrices) is introduced by Taylor's extension and due to this simplicity it is easy to use in any meshfree method. The whole solution domain is divided into non-overlapping cells around each field node as seen in Figure 5.1.
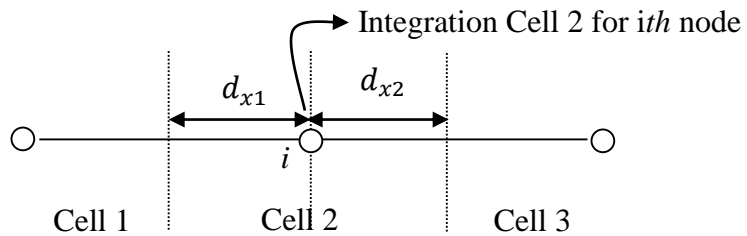
Figure 5. 1. Nodal integration scheme representation

In this thesis, nodal integration scheme is used without high ordered terms of Taylor's expansion for local shear stiffness matrix. This is called as reduced nodal integration scheme. When higher order terms are used in the integration, overly stiff solutions are obtained. This phenomenon is known as "shear locking". Thus, the nodal stiffness matrices can be expressed as:

$$K_f = EI * \begin{cases} \left([B_f]_{x_0}^T * [B_f]_{x_0}\right)(d_{x2} - d_{x1}) + \frac{1}{2!} \cdot \frac{\partial}{\partial x}\left([B_f]_{x_0}^T * [B_f]_{x_0}\right)(d_{x2}^2 - d_{x1}^2) \\ + \frac{1}{3!}\frac{\partial^2}{\partial x^2}\left([B_f]_{x_0}^T * [B_f]_{x_0}\right)(d_{x2}^3 - d_{x1}^3) \end{cases}$$

$$\hspace{11cm} (5.15)$$

$$K_s = GA * \left\{\left([B_s]_{x_0}^T * [B_s]_{x_0}\right)(d_{x2} - d_{x1}) + \frac{1}{2!} \cdot \frac{\partial}{\partial x}\left([B_s]_{x_0}^T * [B_s]_{x_0}\right)(d_{x2}^2 - d_{x1}^2)\right\}$$

5.3. Incremental Solution

In elasto-plastic nonlayered Timoshenko beam analysis, the total load is applied incrementally. As mentioned before, when the beam bending moment reaches the yield moment M_0, the whole cross-section and therefore integration domain becomes plastic.

In solution, *tangential stiffness algorithm* [51] is used. According to load increment, the beam is initially deformed elastically with flexural rigidity *EI*. After yielding, beam shows linear strain hardening and is deformed with $(EI)_{ep}$ Equation 5.11 while the shear rigidity *GA* is assumed unchanged. At later load increments, Equation 5.4 and Equation 5.5 are recalculated and hence stiffness matrices are also recalculated using strain hardening parameter.

CHAPTER 6

# RESULTS AND DISCUSSION

6.1. Cantilever Beam

In the first case study which was used in [60], a thick cantilever beam in Figure 6.1 is used to test the developed code in MATLAB with an elasto-plastic material of E=200 GPa, σ_y= 250 MPa, ν=0.3 and H'= 200 MPa. A concentrated load with 60 kN is applied on the free end of the beam with ten different increments. Also, results of MATLAB code and ANSYS are compared using 11 regular distributed nodes.
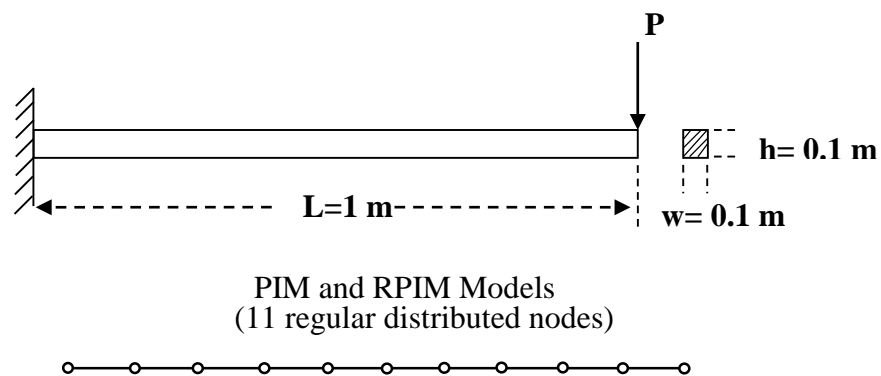

Figure 6. 1. Cantilever beam and its PIM and RPIM models.

In Figure 6.2, the comparison of the elastic displacement distribution for all methods with both high and reduced nodal integration is done. However, for PIM method, higher terms in nodal integration does not affect the solution, for RPIM method solution convergency decreases when higher term of nodal integration is used. The elastic displacement distributions are all good agreement for all methods as shown in Figure 6.3. Normal stress distributions of the beam can be seen in Figure 6.4, they are also all good agreement for all methods. The support domain size has no significant effect on the results for PIM and RPIM with Gauss integration scheme as shown in Figure 6.5 and Figure 6.7. However, it has significant effect for both methods with nodal integration scheme as shown in Figure 6.6 and Figure 6.8. The effect of shape parameters α_c and q are shown in Figures 6.9- 6.12. Shape parameter α_c has no significant effect on the displacement distribution. On the otherhand, shape parameter
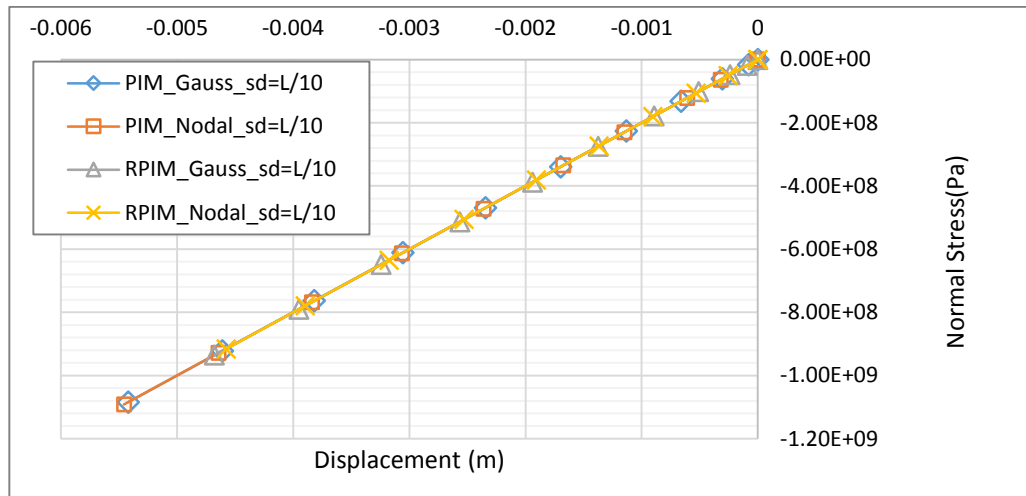
*q* gives only acceptable result when its value approaches 1 as seen in Figures 6.11 and 6.12.
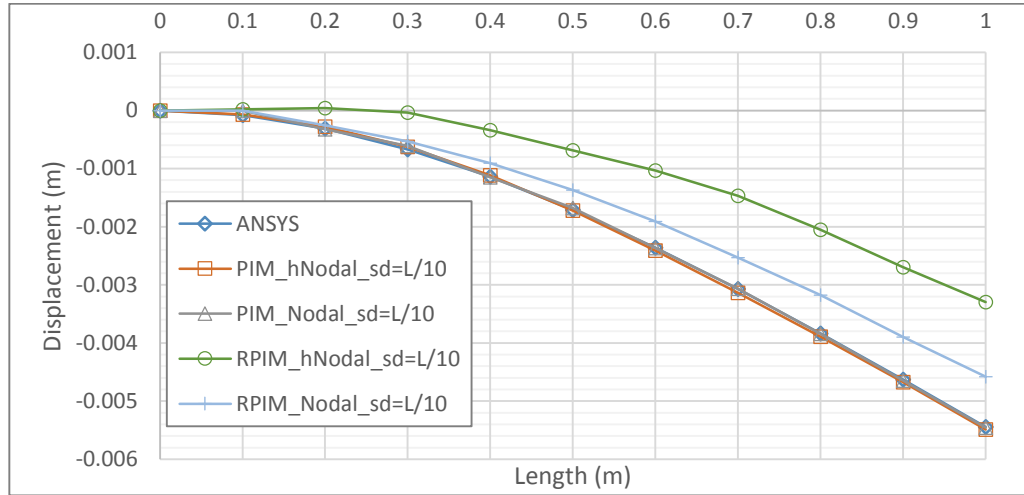
Figure 6. 2. Comparison of solution accuracy for PIM and RPIM with nodal integration with high terms (hNodal) and reduced nodal integration method.
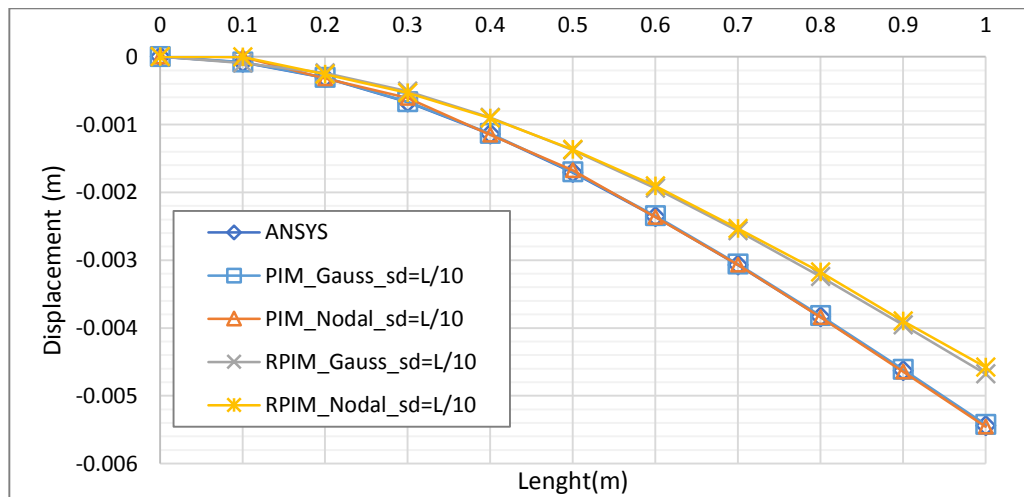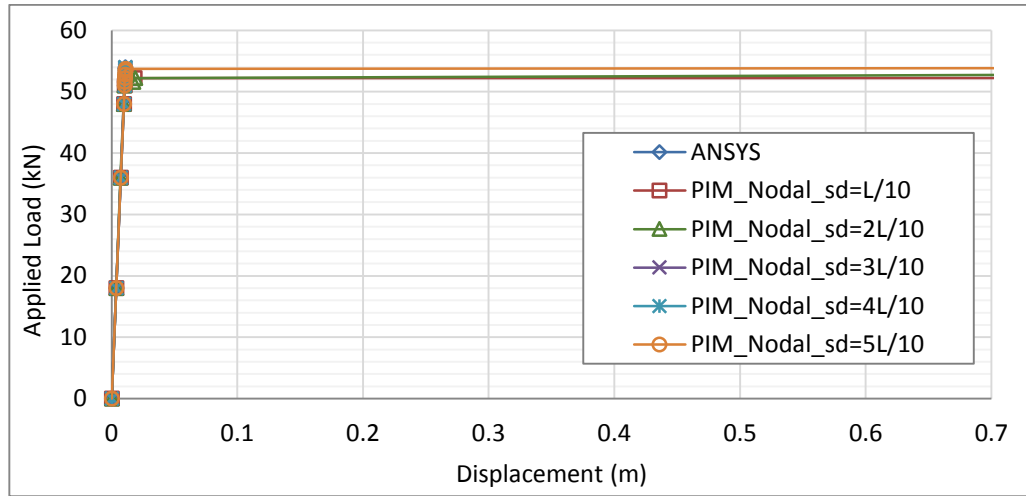

Figure 6. 3. Displacement distribution of cantilever beam along the neutral axis at load increment P=27.0 kN (sd=L/10, α_c=3, *q*=1)

Figure 6. 4. Normal stress distribution of cantilever beam at load increment P=27.0 kN (sd=L/10, α_c=3, q=1)
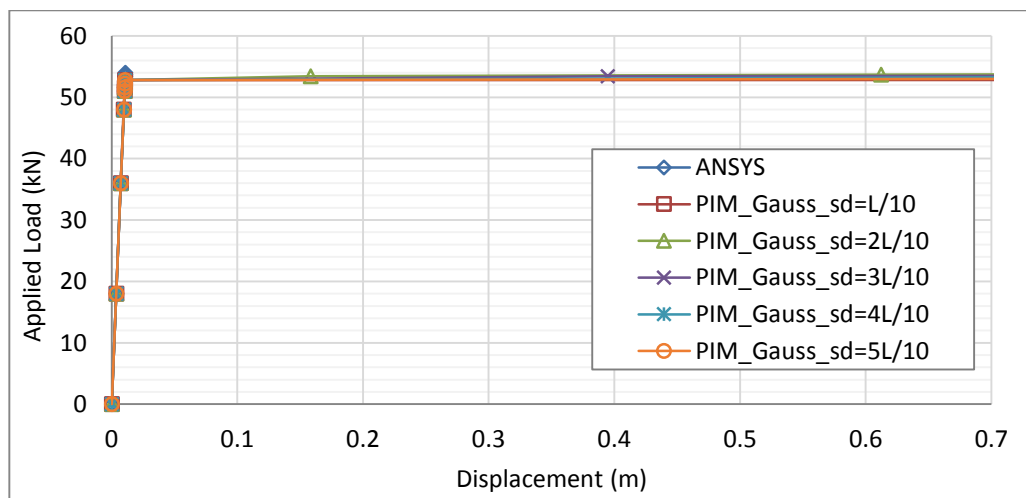
Figure 6. 5. Convergency of the PIM solutions of cantilever beam after yield point for various support domain sizes with Gauss integration scheme.
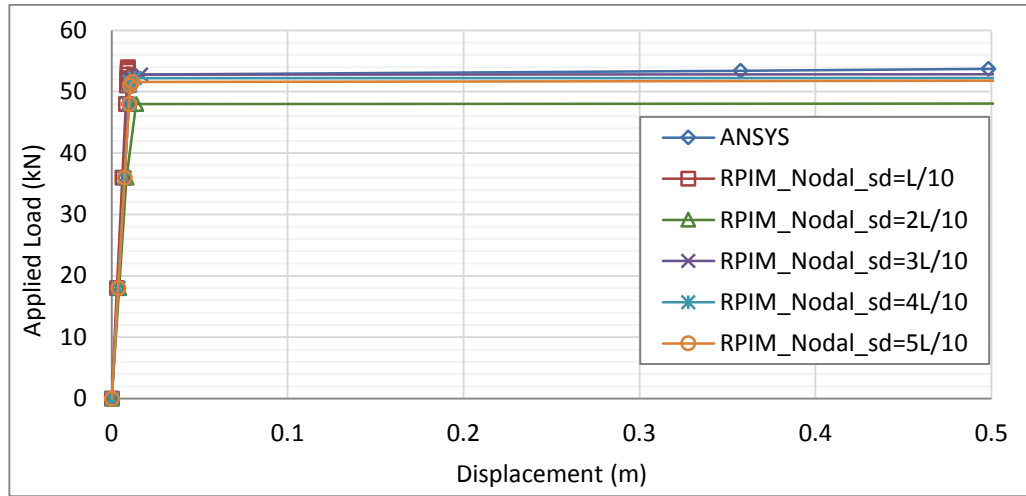
Figure 6. 6. Convergency of the PIM solutions of cantilever beam after yield point for various support domain sizes with nodal integration scheme.
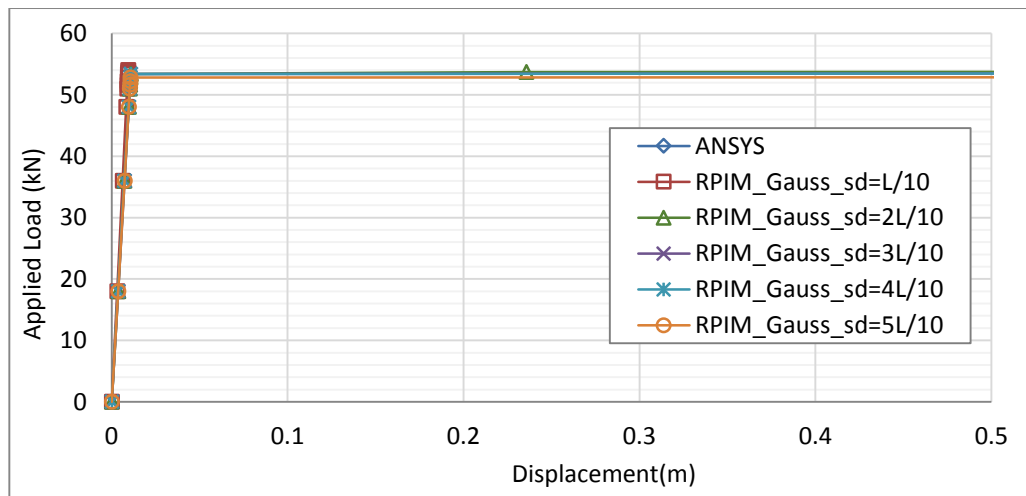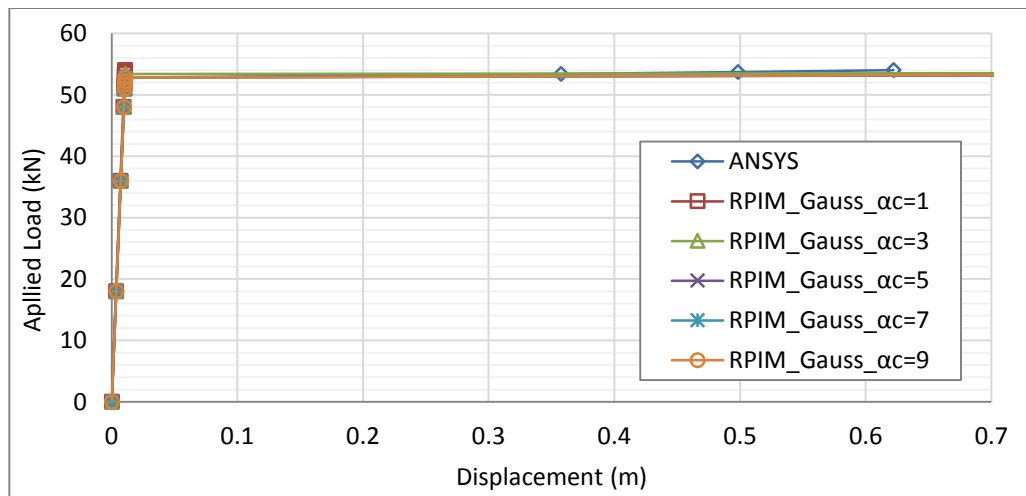

Figure 6. 7. Convergency of the RPIM solutions of cantilever beam after yield point for various support domain sizes with $\alpha_c=3$, $q=1$ and Gauss integration scheme
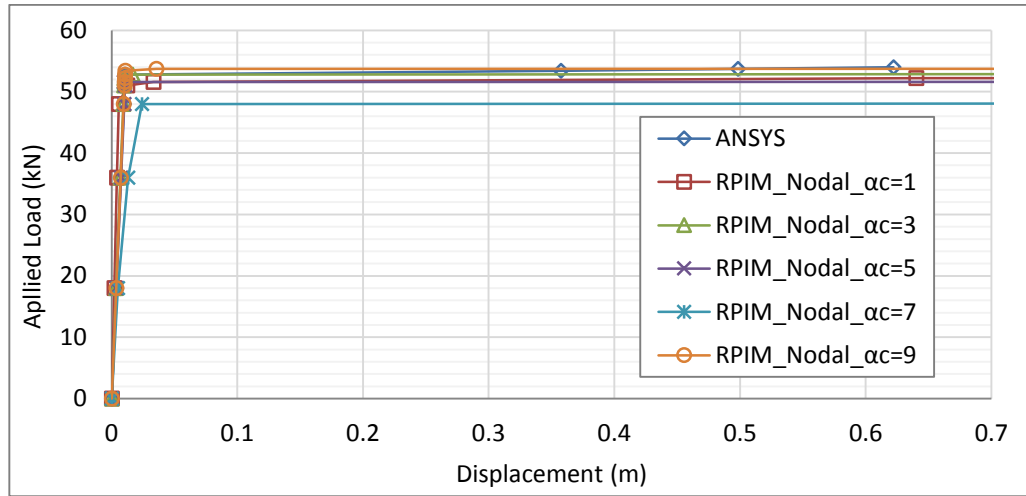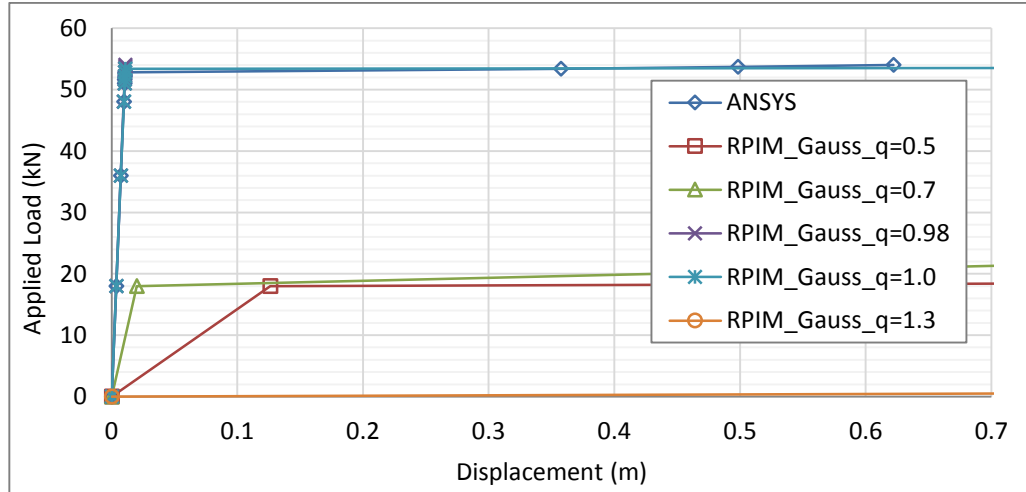
Figure 6. 8. Convergency of the RPIM solutions of cantilever beam after yield point for various support domain sizes with $\alpha_c=3$, $q=1$ and nodal integration scheme.
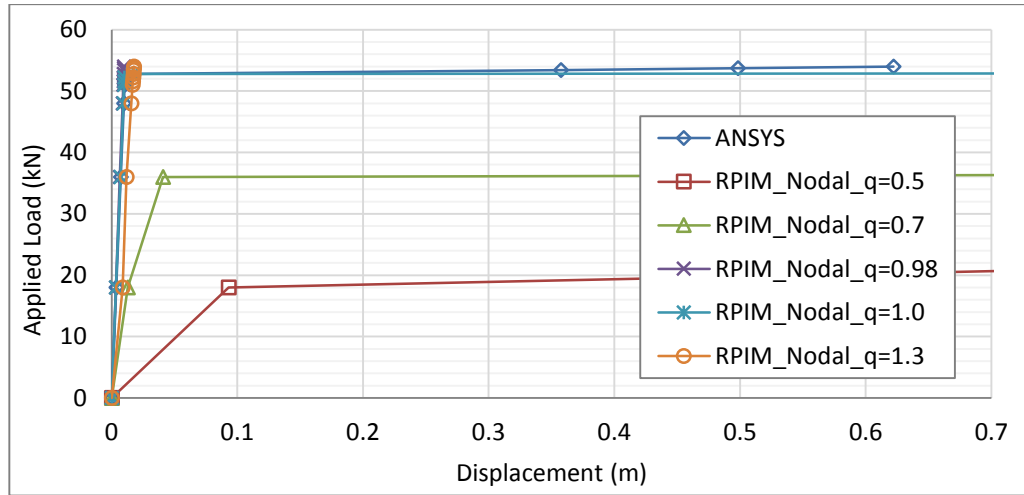

Figure 6. 9. Convergency of the RPIM solutions of cantilever beam after yield point for various α_c shape parameter with sd=3L/10, $q=1$ and Gauss integration scheme.

Figure 6. 10. Convergency of the RPIM solutions of cantilever beam after yield point for various α_c shape parameter with sd=3L/10, q=1 and nodal integration scheme.
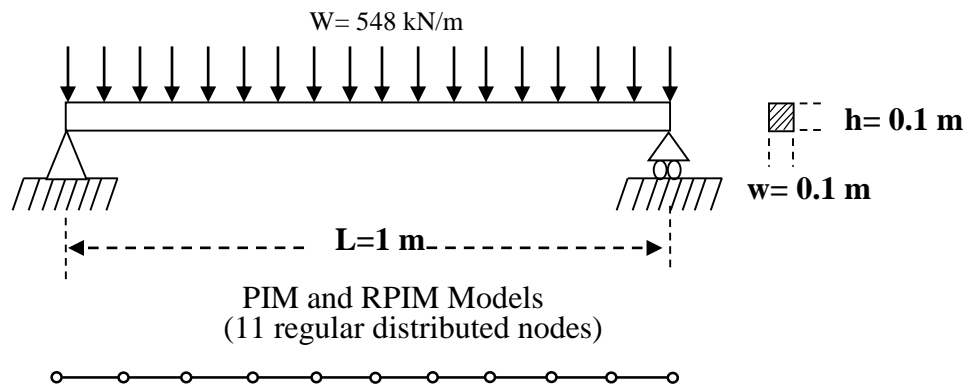

Figure 6. 11. Convergency of the RPIM solutions of cantilever beam after yield point for various q shape parameter with sd=3L/10, α_c=3 and Gauss integration scheme.

Figure 6. 12. Convergency of the RPIM solutions of cantilever beam after yield point for various q shape parameter with sd=3L/10, α_c=3 and nodal integration scheme.
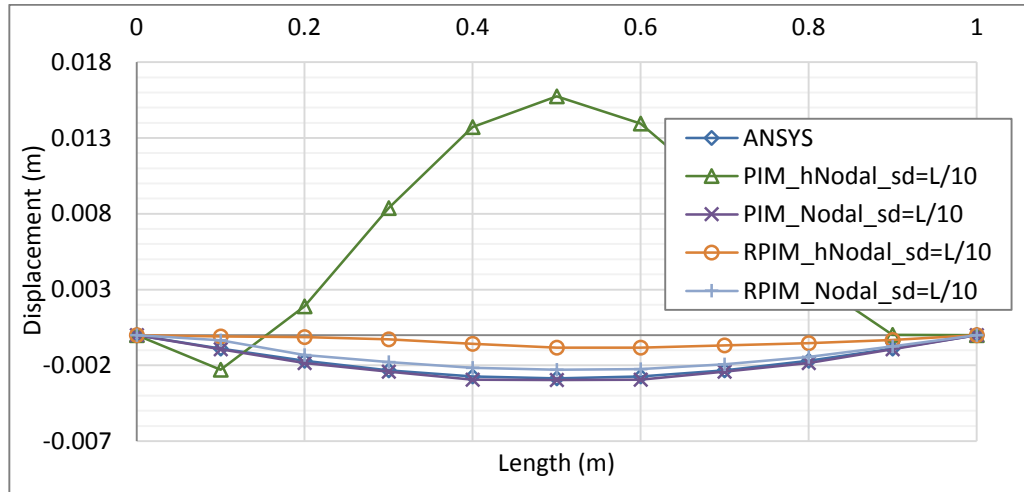
6.2. Simply Supported Beam

**Figure 6. 13.** Simply supported beam and its PIM and RPIM models.

A thick simply supported beam in Figure 6.13 is used to test the developed code in MATLAB with an elasto-plastic material of E=200 GPa, σ_y= 250 MPa, ν=0.3 and H'= 200 MPa. A distributed load with 548 kN/m is applied on the beam with ten different increments. And 11 regular distributed nodes are used to model PIM and RPIM solutions. Also, results of MATLAB code and ANSYS are compared.

In Figure 6.14, the elastic displacement distribution for all methods with both high ordered and reduced nodal integration is investigated. Solution is not acceptable when higher terms are used in integration, but when reduced integration is used, solution becomes acceptable. In Figure 6.15, displacement distribution of the beam is examined for PIM and RPIM methods with Gauss and nodal integration scheme respectively in elastic range. The displacement distribution of the beam is in good agreement for PIM,

31

RPIM with Gauss integration and ANSYS solutions; however displacement distribution for PIM and RPIM with nodal integration scheme has not got accurate solutions. In Figure 6.16, maximum normal stress magnitudes for given load have been shown, and they are in good agreement for all methods. In Figures 6.17-6.18, convergency of the PIM solution with both integration schemes for various support domain sizes is examined. In Figures 6.19-6.20, convergency of the RPIM solution with both integration schemes for various support domain sizes is examined also. In Figures 6.21- 6.22, convergency of the RPIM solution is examined for different α_c shape parameter with both Gauss and nodal integration schemes with 3L/10 support domain size and shape parameter $q=1.0$. In elastic range, α_c shape parameter shows no effect on the convergency of deformation in Gauss integration scheme. In nodal integration, shape parameter α_c gives acceptable results when α_c is 3 and 9. Also in Figures 6.23- 6.24, the effect of shape parameter q on the convergency of RPIM solution is examined and when the q value is near and equal to 1, solution becomes acceptable.


Figure 6. 14. Comparison of solution accuracy for PIM and RPIM with nodal integration with high terms (hNodal) and reduced nodal integration method.
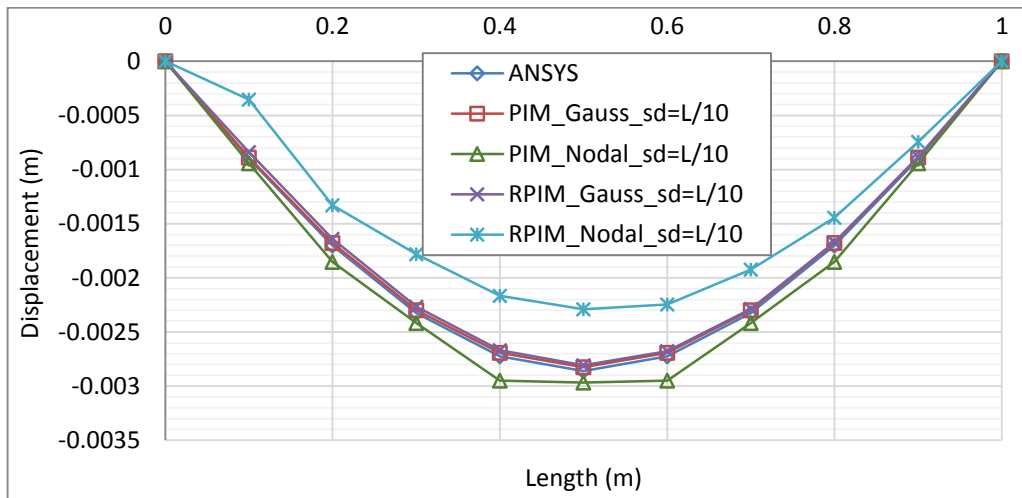
Figure 6. 15. Displacement distribution of simply supported beam along the neutral axis at load increment P=360 kN/m. (sd=L/10, α_c=3, q=1)
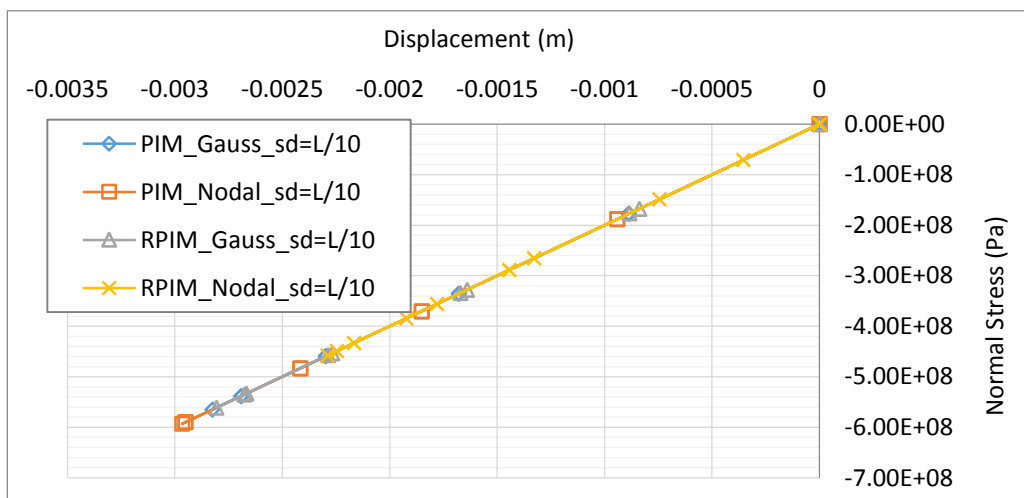
Figure 6. 16. Normal stress distribution of simply supported beam at load increment P=360 kN/m. (sd=L/10, α_c=3, q=1)
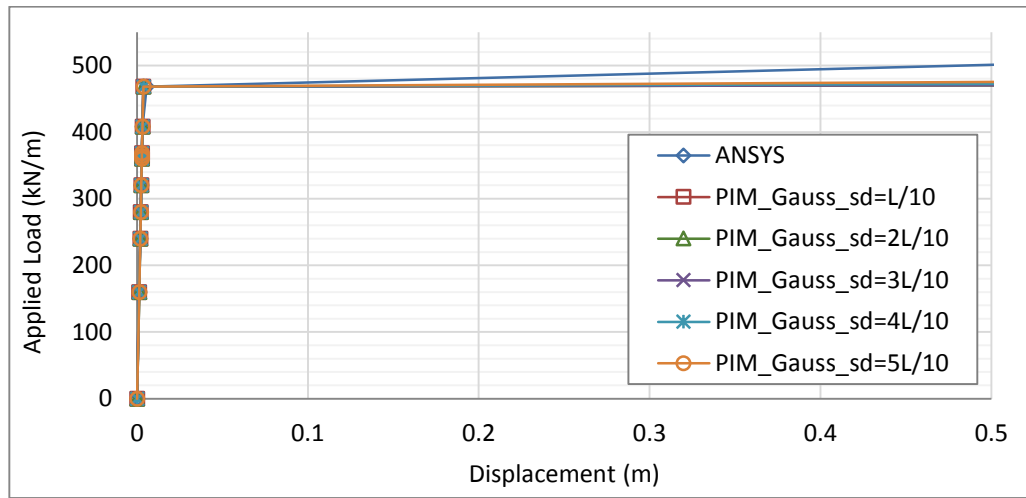
Figure 6. 17. Convergency of the PIM solutions of simply supported beam after yield point for various support domain sizes with Gauss integration scheme.
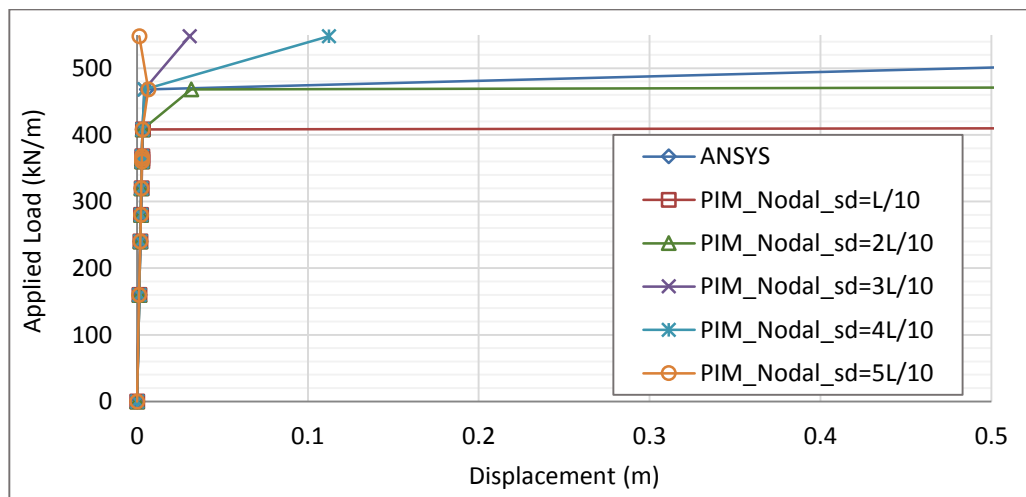
Figure 6. 18. Convergency of the PIM solutions of simply supported beam after yield point for various support domain sizes with nodal integration scheme.
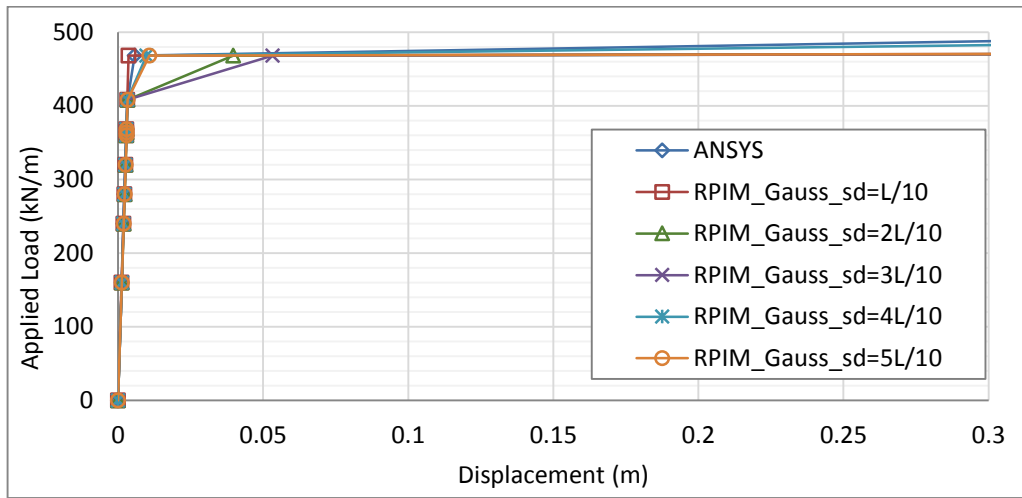
Figure 6. 19. Convergency of the RPIM solutions of simply supported beam after yield point for various support domain sizes with Gauss integration scheme.

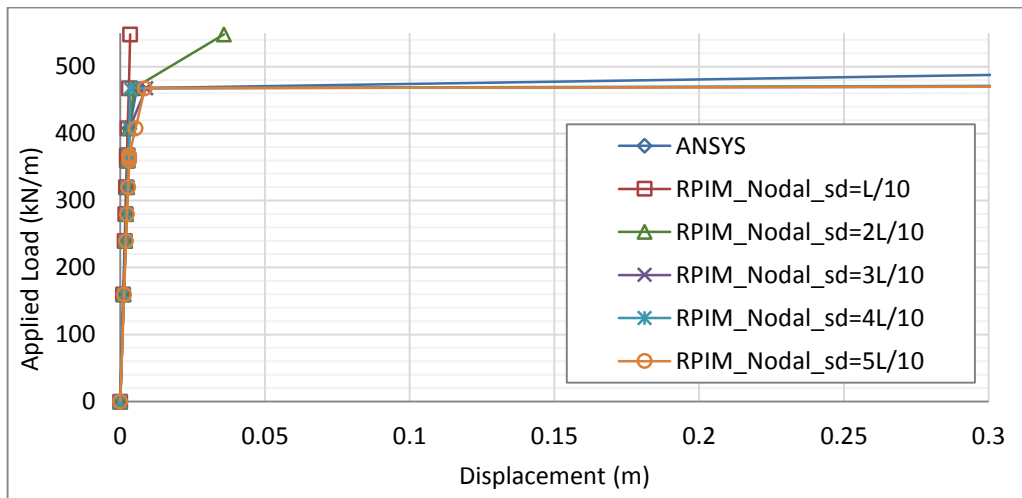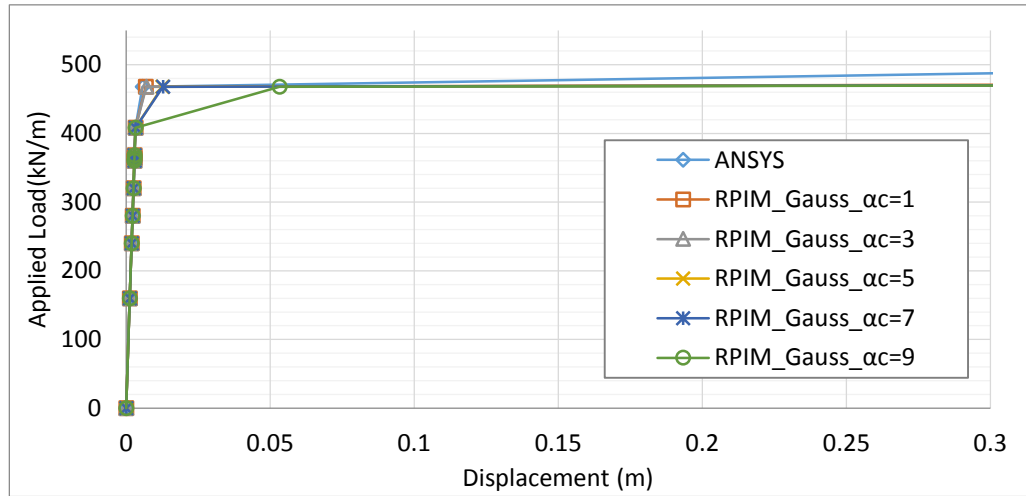**Figure 6. 20.** Convergency of the RPIM solutions of simply supported beam after yield point for various support domain sizes with nodal integration scheme.

Figure 6. 21. Convergency of the RPIM solutions of simply supported beam after yield point for various α_c shape parameter with sd=3L/10, q=1 and Gauss integration scheme.
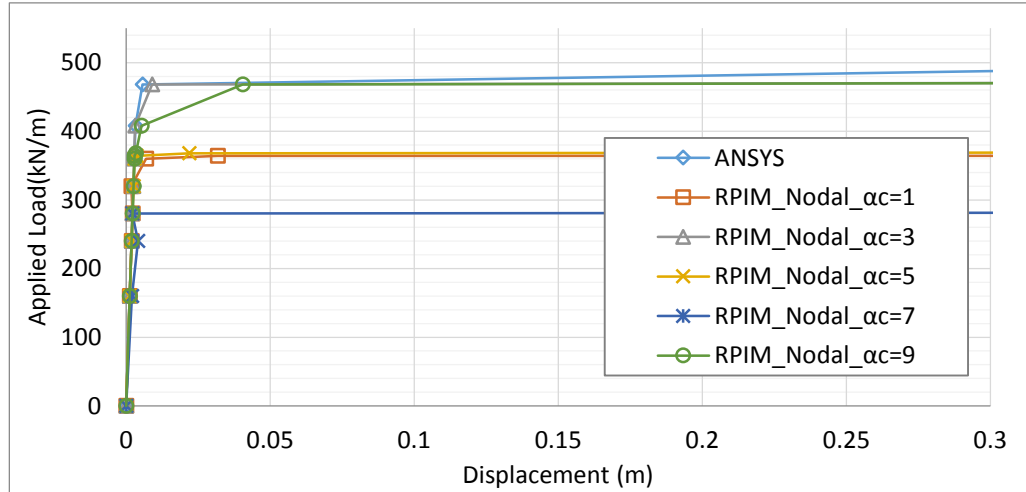
Figure 6. 22. Convergency of the RPIM solutions of simply supported beam after yield point for various α_c shape parameter with sd=3L/10, q=1 and nodal integration scheme.

Figure 6. 23. Convergency of the RPIM solutions of simply supported beam after yield point for various q shape parameter with sd=3L/10, α_c=3 and Gauss integration scheme.
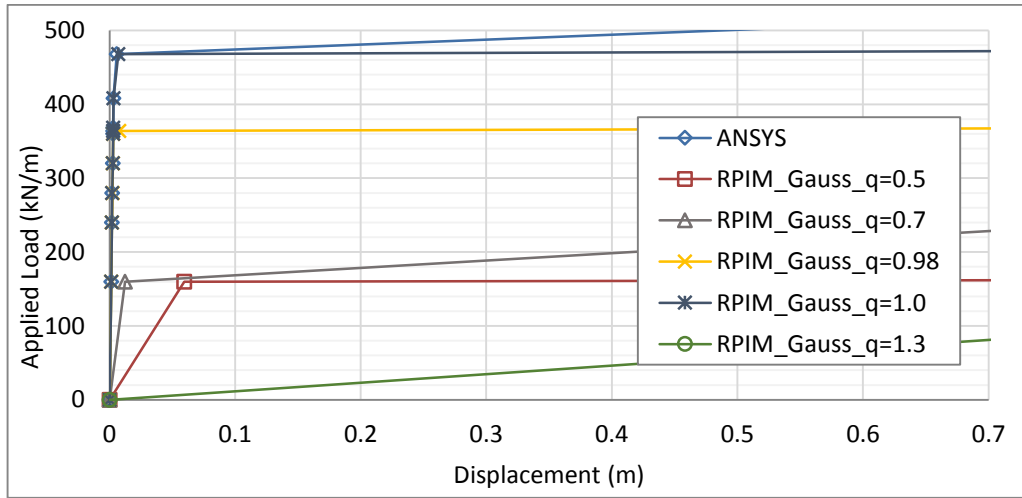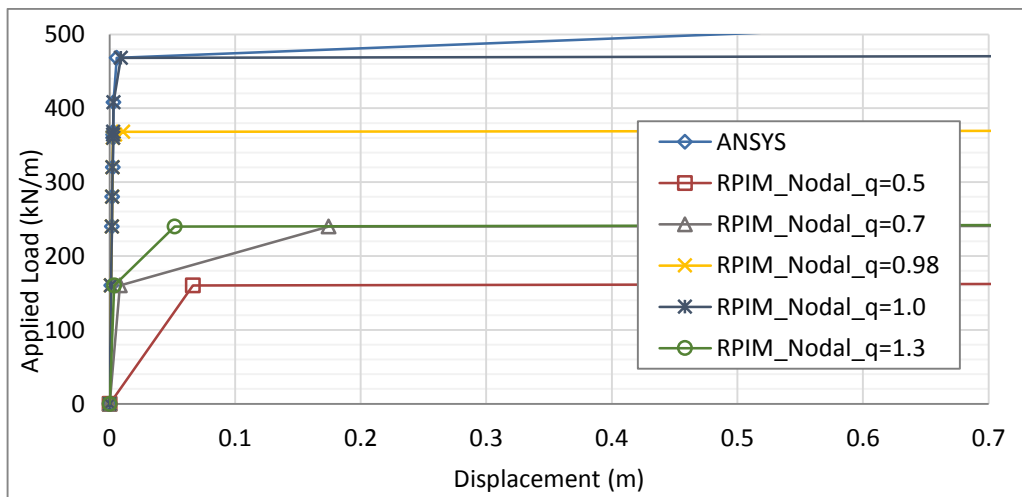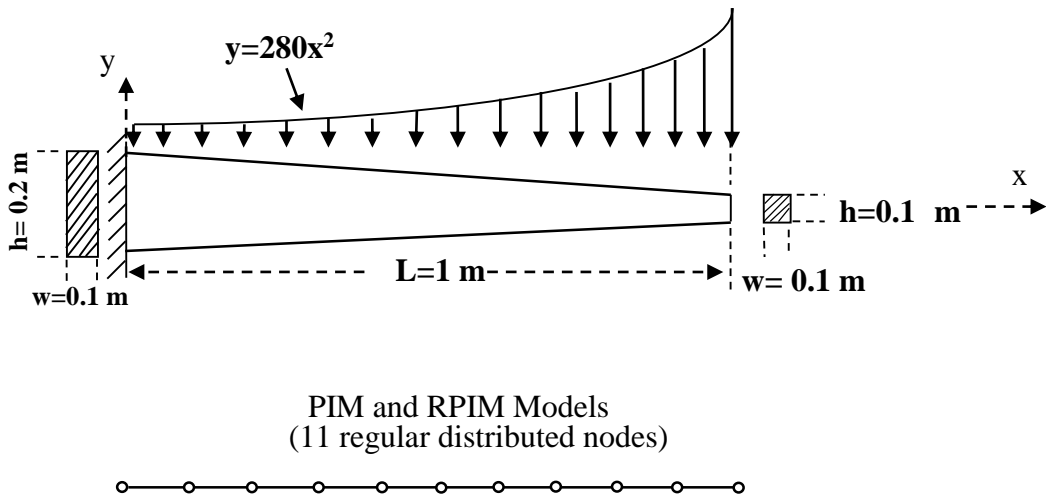

Figure 6. 24. Convergency of the RPIM solutions of simply supported beam after yield point for various q shape parameter with sd=3L/10, α_c=3 and nodal integration scheme.
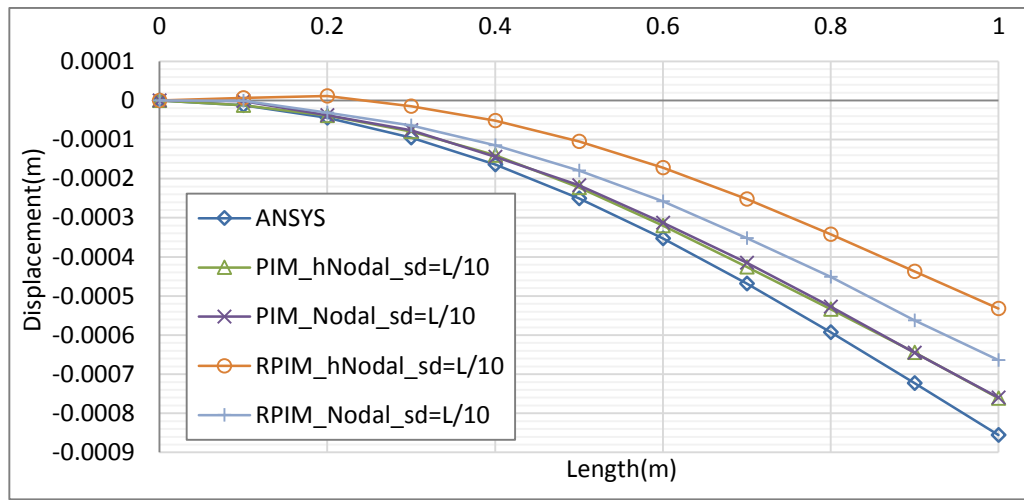
6.3. Tapered Cantilever Beam

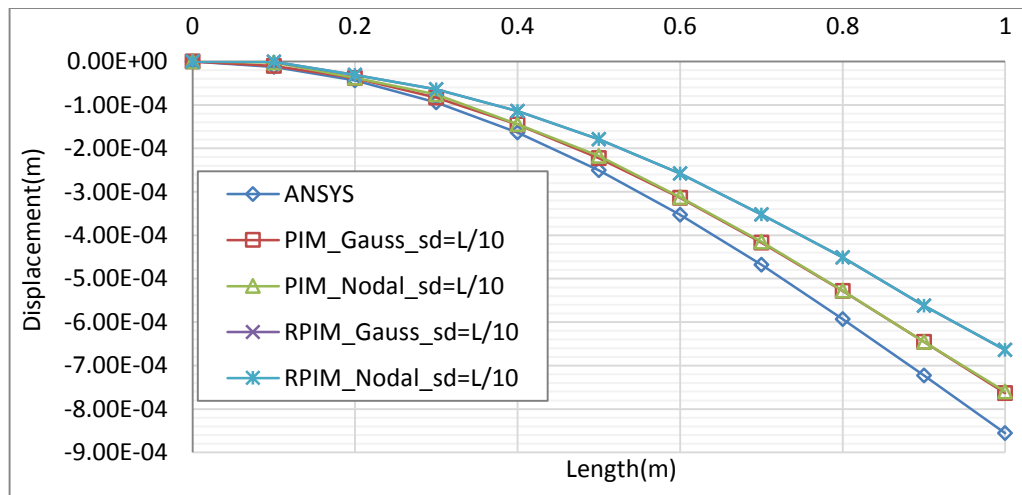**Figure 6. 25.** Tapered cantilever beam with parabolic distributed load and its PIM and RPIM models.

A thick, tapered cantilever beam with own weight and parabolic distributed load ($y=280x^2$ kN/m) is used as a third case. The beam in Figure 6.25 is a structural steel which has a density of 7850 kg/m^3, young's modulus E of 200 GPa ,yield strength σ_y of 50 MPa, $v=0.3$ and $H'=200$ MPa. A distributed load ($y=280x^2$ kN/m) is applied on the beam with ten different increments. And 11 regular distributed nodes are used to model PIM and RPIM solutions. Also, the results of generated source code and ANSYS are compared.

In Figure 6.26, the elastic displacement distribution for all methods with both high ordered and reduced nodal integration is investigated. For PIM with both high ordered and reduced nodal integration schemes, the solution accuracy is not affected. But for RPIM, when high ordered nodal integration scheme is used, the solution includes some errors. Displacement distribution of the beam is examined for PIM and RPIM methods with Gauss and nodal integration scheme respectively in elastic range in Figure 6.27. The displacement distribution of the beam is in good agreement for all methods. In Figure 6.28, maximum normal stress magnitudes for given load have been shown, and they are in good agreement for all methods. In Figures 6.29-6.30, convergency of the PIM with both integration schemes solution for various support domain sizes is examined. And in Figures 6.31- 6.32, convergency of the RPIM solution with both integration schemes for various support domain sizes is examined. For different support domains, PIM with both integration schemes shows good agreement; however

RPIM with both integration methods gives accurate results after support domain size 0.2. Additionally, convergency of the RPIM solution is examined for different α_c shape parameter with both Gauss and nodal integration schemes in Figure 6.33 and Figure 6.34. In elastic range, α_c shape parameter has no effect on the convergency of displacement. Also in Figure 6.35 and Figure 6.36, the effect of shape parameter q on the convergency of RPIM solution is examined and when the q value is near to 1, solution becomes acceptable.

Figure 6. 26. Comparison of solution accuracy for PIM and RPIM with nodal integration with high terms (hNodal) and reduced nodal integration method.

Figure 6. 27. Displacement distribution of tapered cantilever beam along the neutral axis for the distributed load $y=100x^2$ kN/m (sd=L/10, α_c=3, q=1).
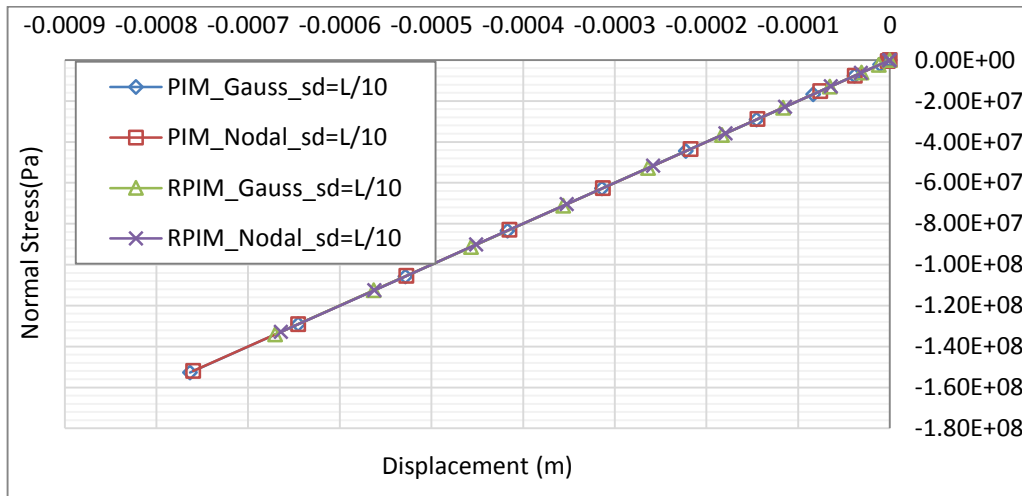
Figure 6. 28. Normal stress distribution of tapered cantilever beam for the distributed load $y=100x^2$ kN/m (sd=L/10, α_c=3, q=1).
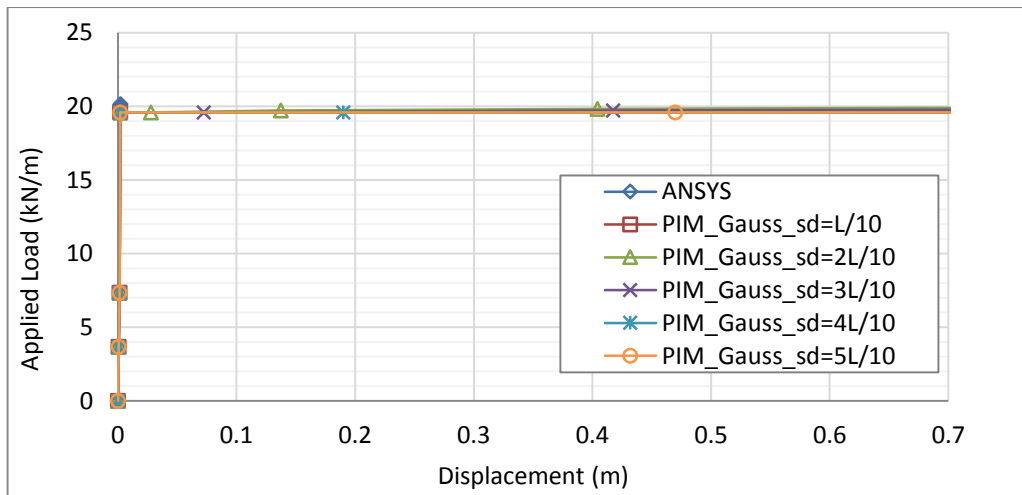
Figure 6. 29. Convergency of the PIM solution of tapered cantilever beam after yield point for various support domain sizes with Gauss integration scheme.
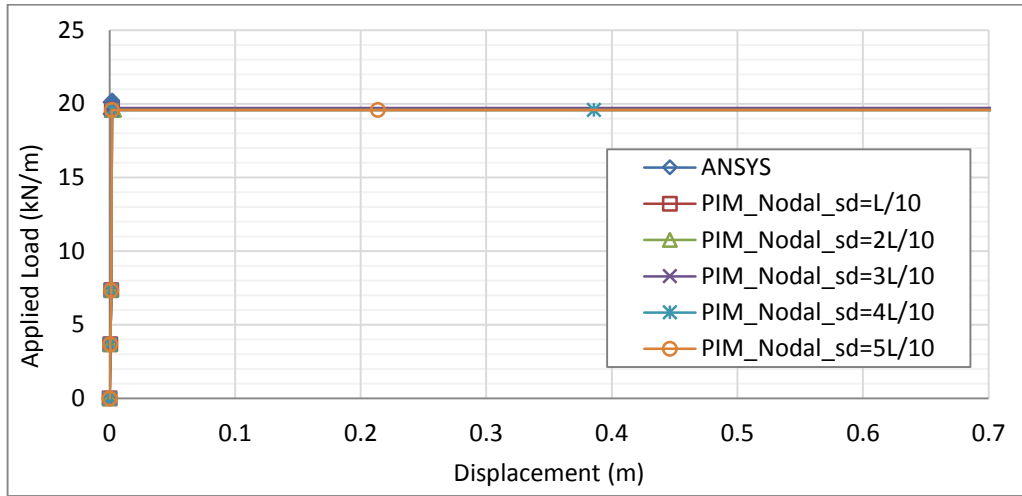
Figure 6. 30. Convergency of the PIM solution of tapered cantilever beam after yield point for various support domain sizes with nodal integration scheme.
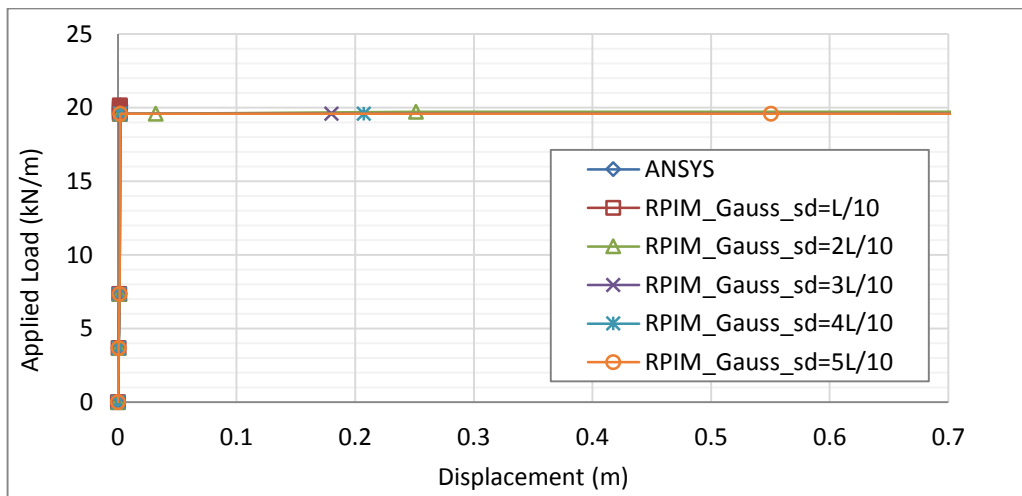
Figure 6. 31. Convergency of the RPIM solution of tapered cantilever beam after yield point for various support domain sizes with q=1, α_c=3 and Gauss integration scheme.
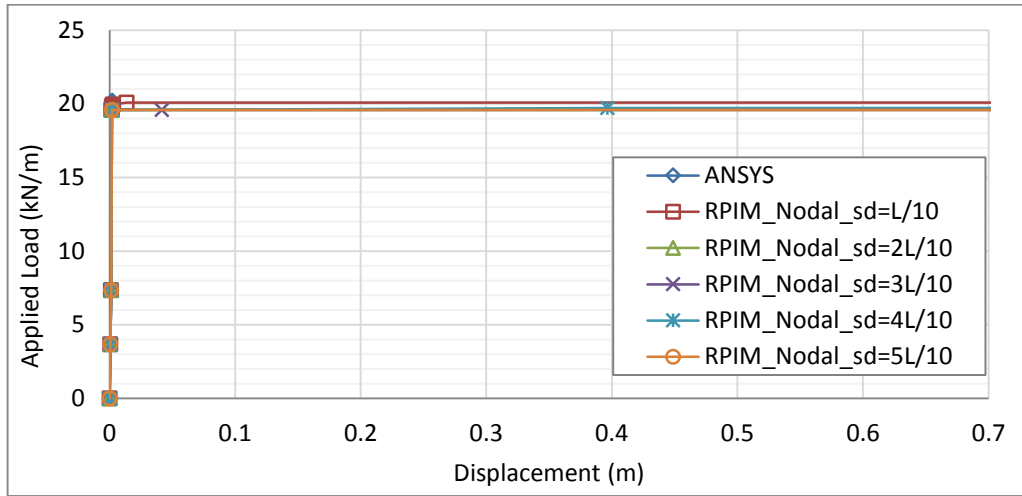
Figure 6. 32. Convergency of the RPIM solution of tapered cantilever beam after yield point for various support domain sizes with $q=1$, $\alpha_c=3$ and nodal integration scheme.
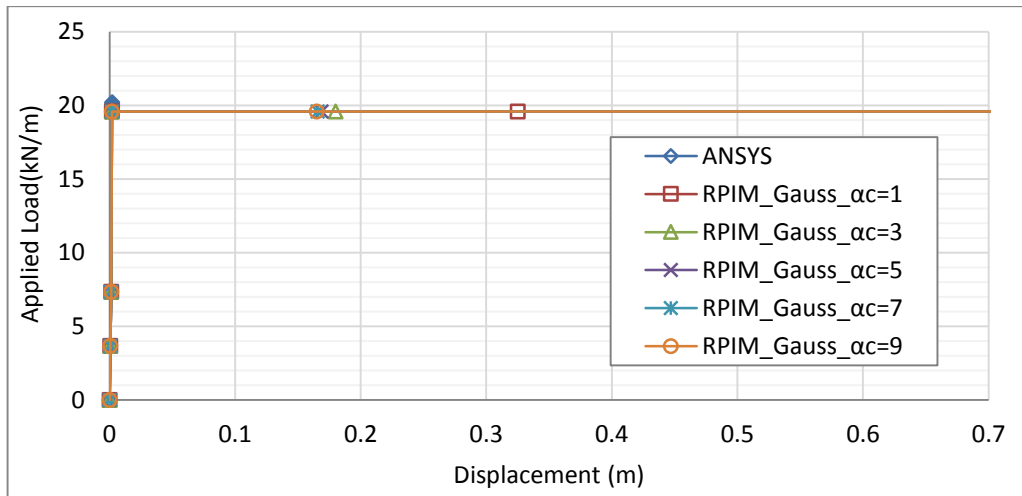
Figure 6. 33. Convergency of the RPIM solution of tapered cantilever beam after yield point for various α_c with sd=3L/10, $q=1$ and Gauss integration scheme.

Figure 6. 34. Convergency of the RPIM solution of tapered cantilever beam after yield point for various α_c with sd=3L/10, q=1 and nodal integration scheme.
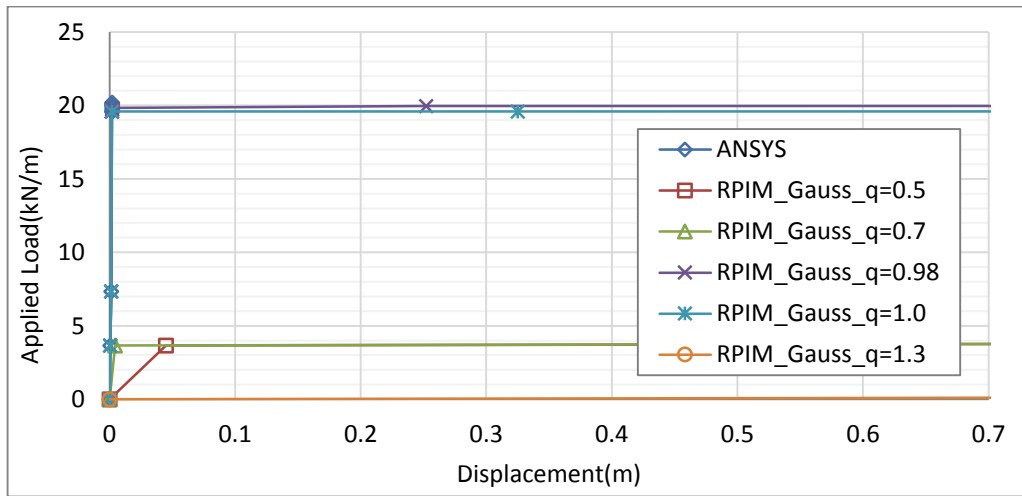
Figure 6. 35. Convergency of the RPIM solution of tapered cantilever beam after yield point for various q with sd=3L/10, α_c=3 and Gauss integration scheme.

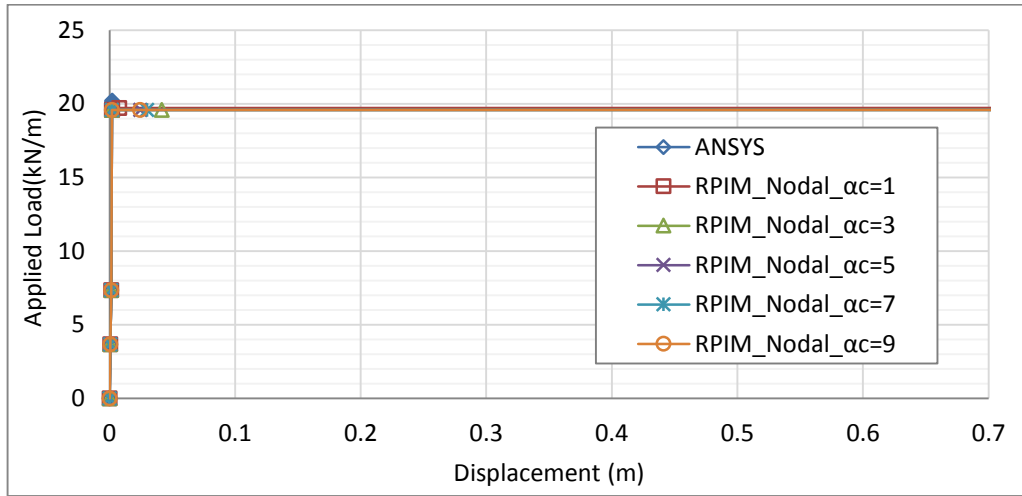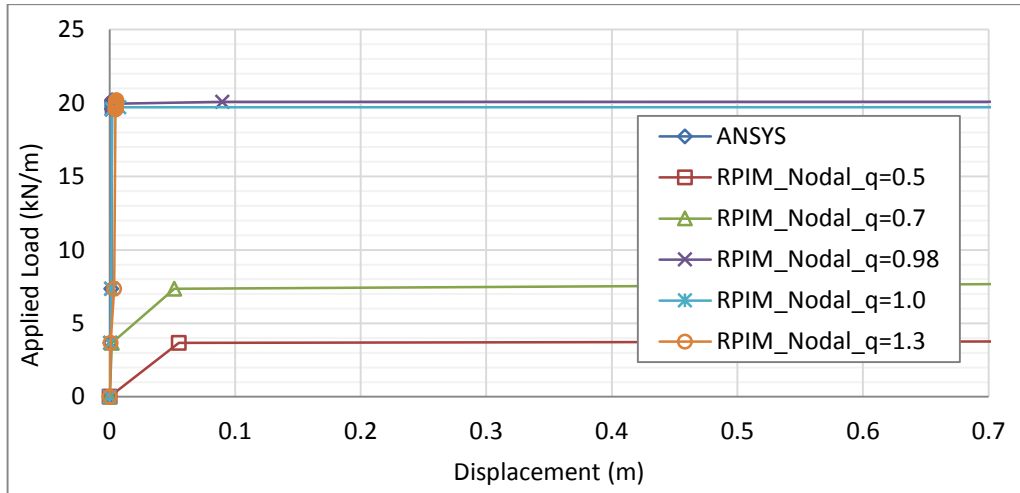**Figure 6. 36.** Convergency of the RPIM solution of tapered cantilever beam after yield point for various *q* with sd=3L/10, α$_c$=3 and nodal integration scheme.

6.4. Constant Strength Simply Supported Beam
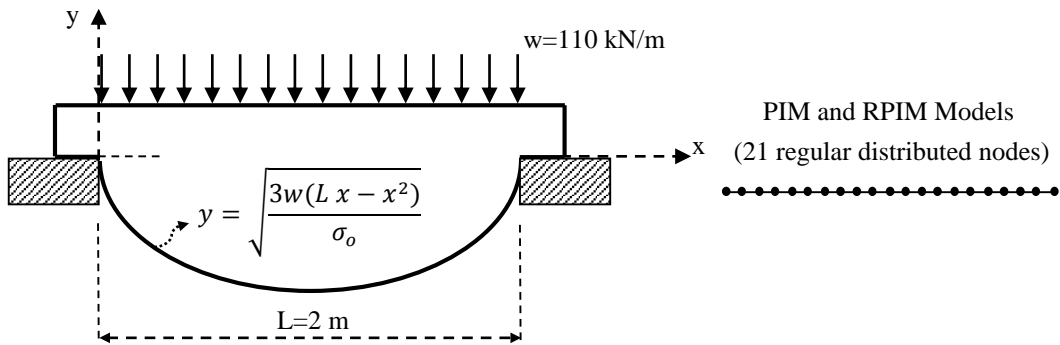
Figure 6. 37. Constant strength simply supported beam and its PIM and RPIM models.

A constant strength simply supported beam in Figure 6.37 with elasto-plastic material of young's modulus E is 200 GPa, yield strength σ_y is 50 MPa, ν=0.3 and H'=200 MPa is used as another case problem in this thesis which is published in [61]. A uniformly distributed load of 110 kN/m is applied with ten different increments.

In Figure 6.38, the elastic displacement distribution for all methods with both high ordered and reduced nodal integration is investigated. For PIM with both high ordered and reduced nodal integration schemes, the solution distribution is not affected. For RPIM solutions, when reduced nodal integration scheme is used, solution accuracy is increased. The elastic displacement distributions are all good agreements for all

methods as shown in Figure 6.39. Normal stress distribution of the beam is shown in Figure 6.40, and they are in good agreement for all methods. Convergency of the PIM with both integration schemes for various support domain sizes are shown in Figures 6.41- 6.42. Also, convergency of the RPIM with both integration schemes for various support domain sizes can be seen in Figures 6.43- 6.44. As seen in figures, all methods give accurate results for various support domain sizes. In Figure 6.45 and Figure 6.46, effect of the α_c shape parameter on the solution convergency is examined, and shows no an important effect in RPIM solutions. However, shape parameter q gives acceptable results when it is equal to 1, as seen in Figure 6.47 and Figure 6.48.
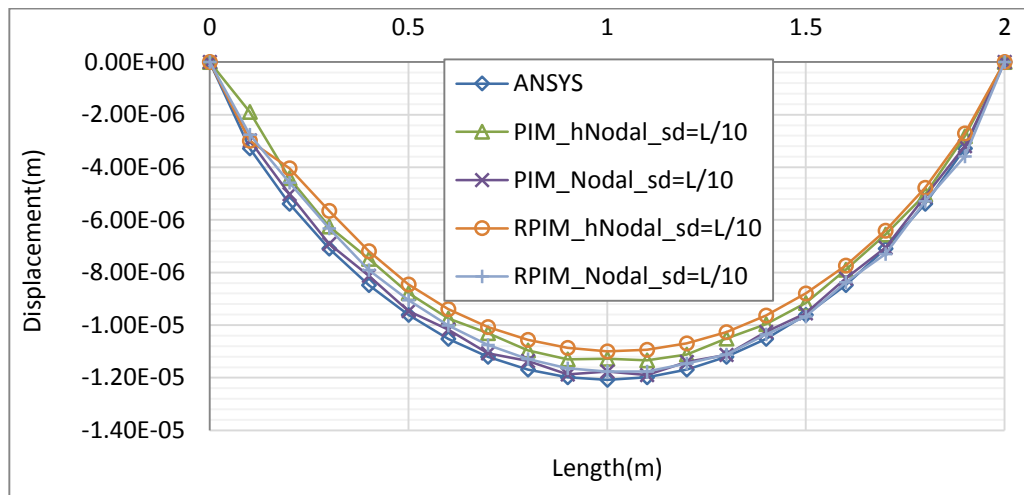
Figure 6. 38. Comparison of solution accuracy for PIM and RPIM with nodal integration with high terms (hNodal) and reduced nodal integration method.
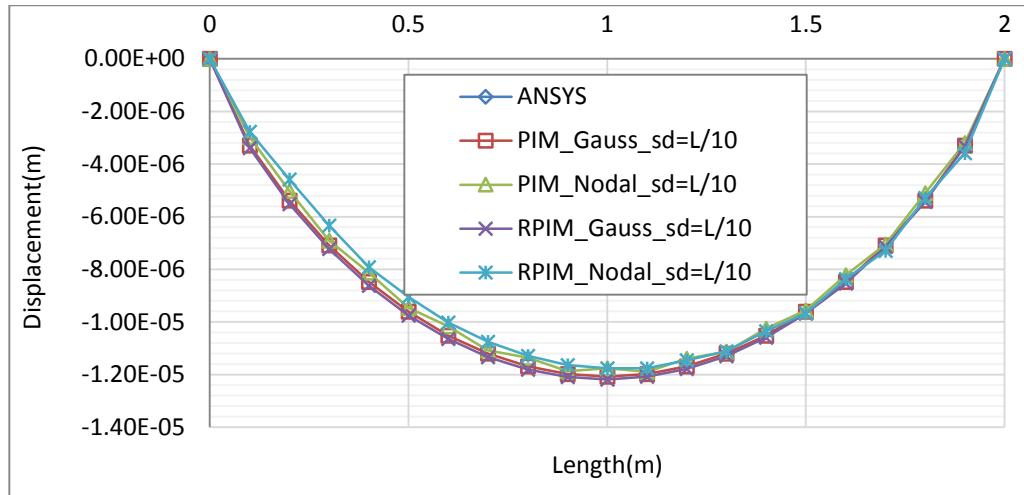
Figure 6. 39. Displacement distribution of constant strenght simply supported beam along the neutral axis at the last load increment (w=100 kN/m, sd=L/10, q=1, α_c=3).
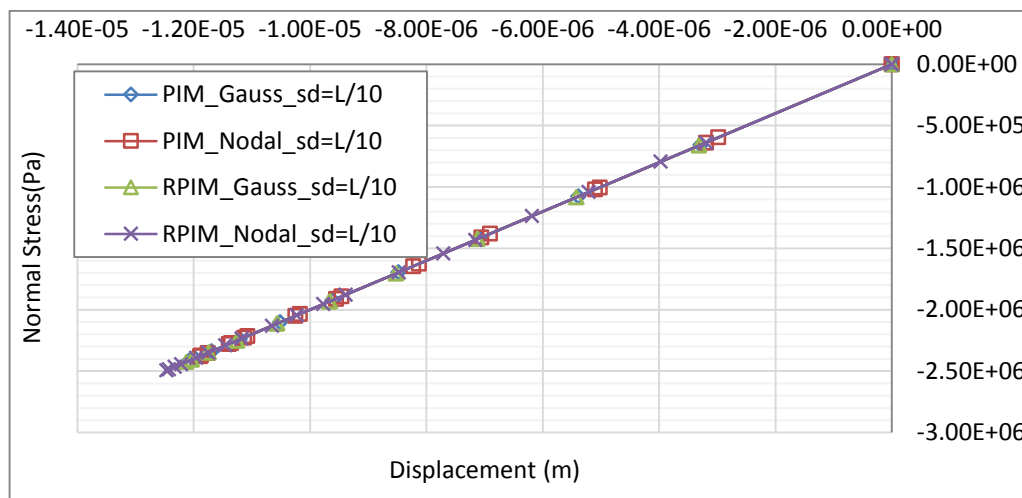
Figure 6. 40. Normal stress distribution of constant strenght simply supported beam at the last load increment (w=100 kN/m, sd=L/10, q=1, α_c=3).
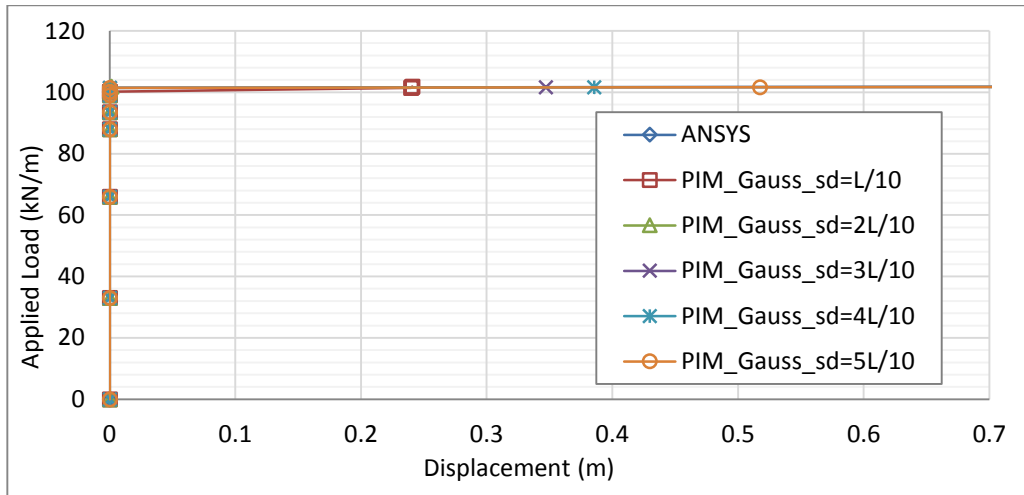
Figure 6. 41. Convergency of the PIM solution of constant strength simply supported beam after yield point for various support domain sizes with Gauss integration scheme.
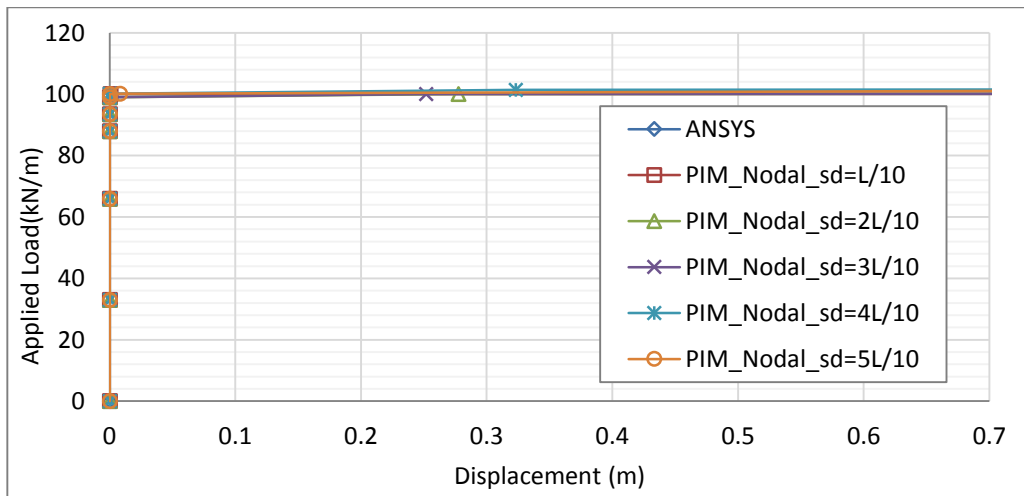
Figure 6. 42. Convergency of the PIM solution of constant strength simply supported beam after yield point for various support domain sizes with nodal integration scheme.
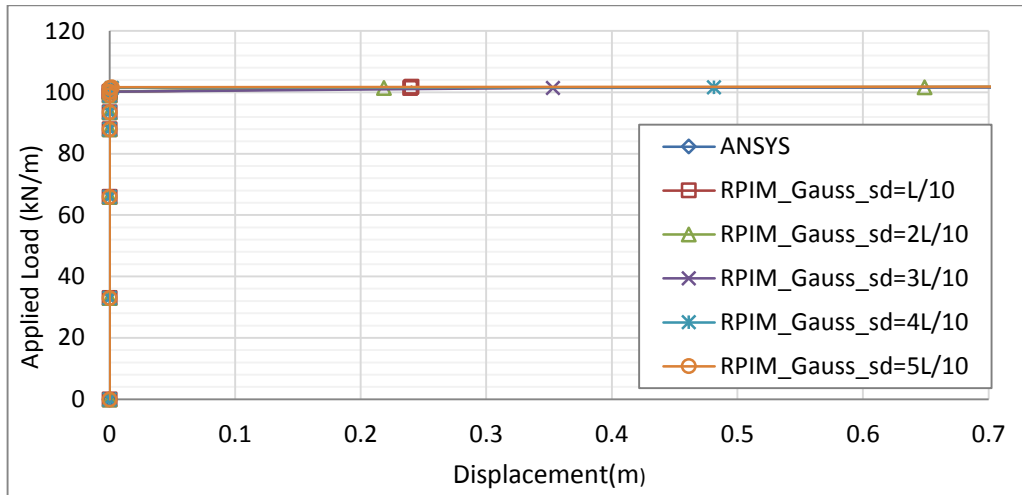
Figure 6. 43. Convergency of the RPIM solution of constant strength simply supported beam after yield point for various support domain sizes with $q=1$, $\alpha_c=3$ and Gauss integration scheme.
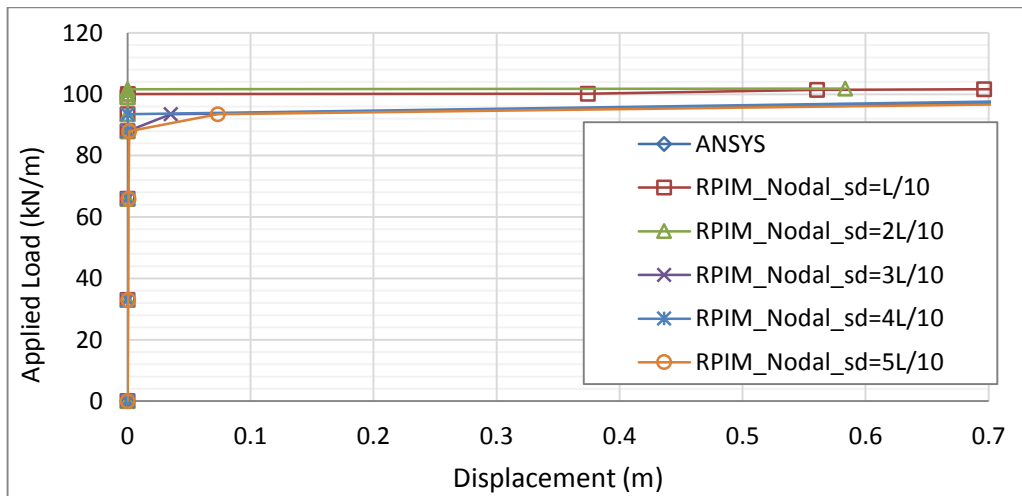
Figure 6. 44. Convergency of the RPIM solution of constant strength simply supported beam after yield point for various support domain sizes with $q=1$, $\alpha_c=3$ and nodal integration scheme.
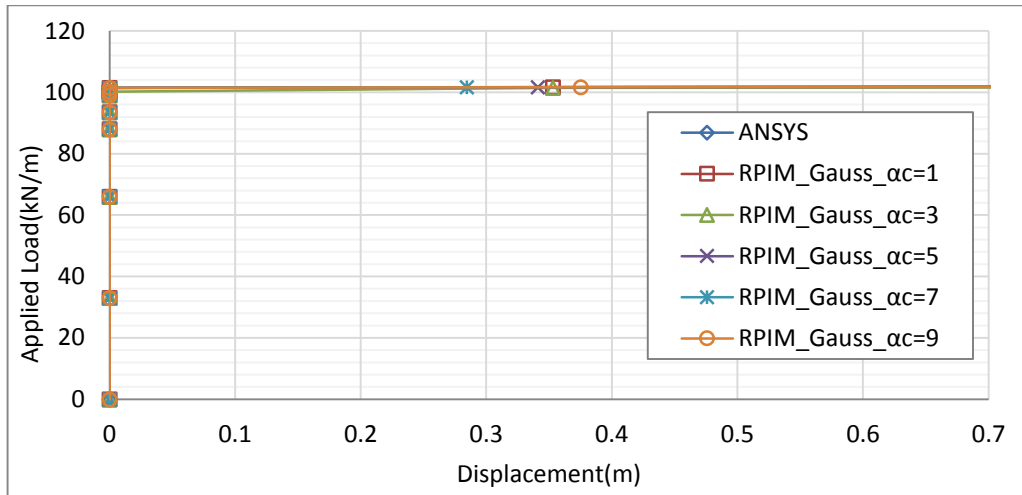
Figure 6. 45. Convergency of the RPIM solution of constant strength simply supported beam after yield point for various α_c parameters with sd=3L/10, q=1 and Gauss integration scheme.
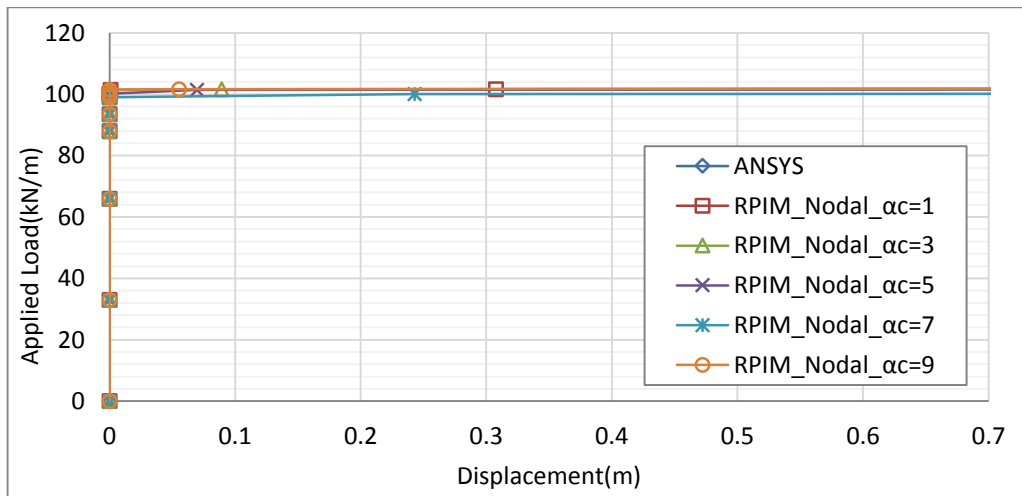
Figure 6. 46. Convergency of the RPIM solution of constant strength simply supported beam after yield point for various α_c parameterswith sd=3L/10, q=1 and nodal integration scheme.
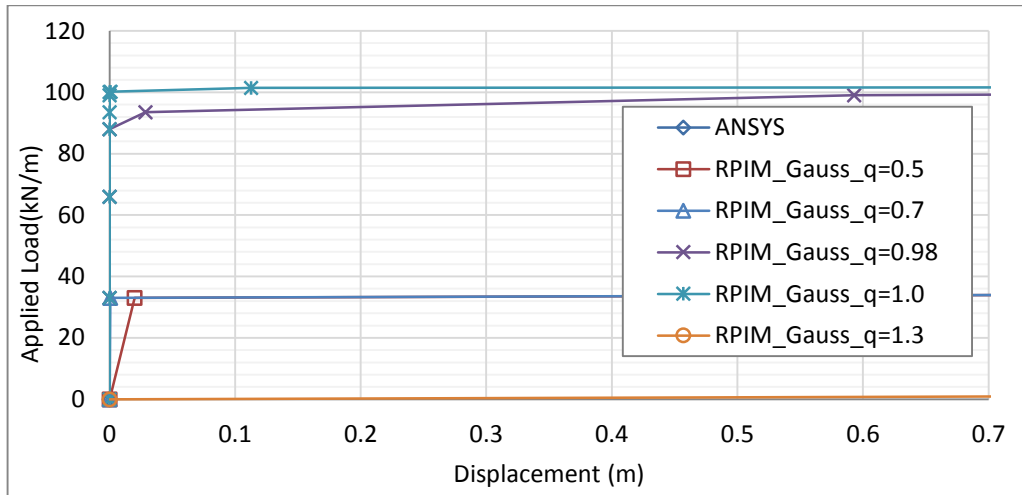
Figure 6. 47. Convergency of the RPIM solution of constant strength simply supported beam after yield point for various q parameters with sd=3L/10, α_c =3 and Gauss integration scheme.
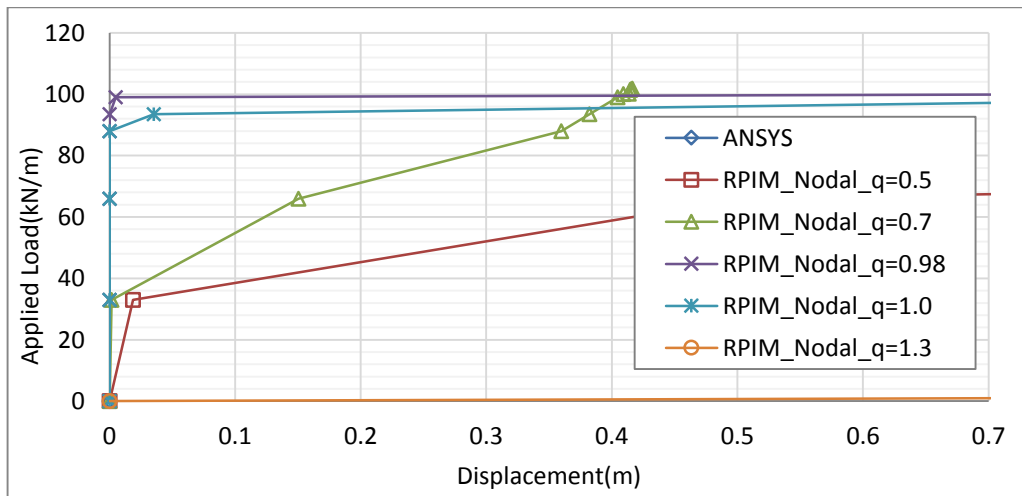
Figure 6. 48. Convergency of the RPIM solution of constant strength simply supported beam after yield point for various q parameters with sd=3L/10, α_c =3 and nodal integration scheme.

CHAPTER 7

CONCLUSION

In this thesis, elasto-plastic analysis of thick beam is presented using PIM and RPIM methods. For this aim, a MATLAB program is written using an algorithm that is improved considering elasto-plastic solution of thick beams using PIM and RPIM methods.

In the original PIM and RPIM solutions, standard Gauss integration scheme is used considering background integration cells. In this approach, to avoid "shear locking" problem, reduced integration scheme is applied. In contrast to standard Gauss integration scheme, in this study, in addition to this, a nodal integration scheme is used based on Taylor series expansion. It removes the necessity of using background integration cells.

When these two integration scheme are compared, it is found that similar "shear locking" problem is observed in the nodal integration solutions. Therefore, in order to avoid this problem, lower order terms are used in the shear stress part of stiffness matrix as in the standard Gauss integration method. Their results are seriously improved and "shear locking" problem is solved.

The results also show that the support domain size does not affect the accuracy for both PIM and RPIM methods when the number of nodes are used between 2 and 11 in a support domain.

Shape parameters of RPIM are also examined, and solutions show that α_c parameter has no a significant effect on the solution accuracy, but when α_c is equal to 3, best results are obtained. For the shape parameter of q, it is obvious that the results are seriously affected by changing its value. The best results are obtained when its value is used around 1.

REFERENCES

[1] Liu G.R. (2010). Meshfree Methods: Moving Beyond the Finite Element Method. 2nd Ed. *CRC Press: Boca Raton*.

[2] Liu G.R., Gu Y.T. (2005). An Introduction to Meshfree Methods and Their Programming. *Springer: Dordrecht, Netherlands*.

[3] Liu G.R., Gu Y.T. (1999). A point interpolation method. *4th Asia-Pacific Conference on Computational Mechanics*, Singapore. 1009-1014.

[4] Liu G.R., Gu Y.T. (2001). A point interpolation method for 2-D solids. *Int. J. Numer. Methods Engrg*, **50**, 937-951.

[5] Liu G.R., Yang K. Y. (1998). A penalty method for enforce essential boundary conditions in element free Galerkin method. The proceeding of the 3rd HPC Asia'98, Singapore, 715-721.

[6] Gosz J., Liu W.K. (1996). Admissible approximations for essential boundary conditions in the reproducing kernel particle method. *Comput. Mech.*, **19**, 120-135.

[7] Günther F.C., Liu W. K. (1998). Implementation of boundary conditions for meshless methods. *Comput. Meth. Appl. Mech. Engrg.* **163**(1-4), 205-230.

[8] Liu G.R., Yang K.Y. (1998). A penalty method for enforcing essential boundary conditions in element free Galerkin method, *Proceedings of the 3rd HPC Asia `98*, Singapore, 715-721.

[9] Liu G.R., Gu Y.T. (2003). A matrix triangularization algorithm for the polynomial point interpolation method, Comput. Meth. Appl. Mech. Engrg. **192**, 2269- 2295.

[10] Wang J.G., Liu G.R. (2002). A point interpolation meshless method based on radial basis functions. *Int. J. Numer. Meth. Engrg.*, **54**, 1623-1648.

[11] Kanber B., Bozkurt O.Y. (2008). A diagonal offset algorithm for the polynomial point interpolation method. *Commun. Numer. Meth. Engng.,* **24**(12), 1909–1922.

[12] Gu Y.T. and Liu G.R. (2001). A local point interpolation method for static and dynamic analysis of thin beams. *Comput. Methods Appl. Mech. Engrg*. **190**, 5515-5528.

[13] Boyd J.P. (1985). Complex coordinate methods for hydrodynamic instabilities and Stum-Liouville Eigen problems with an interior singularity. *J. of Comp. Physcs*, **57**, 454- 471.

[14] Liu G.R., Zhang G.Y, Gu Y.T. and Wang Y.Y. (2005). A meshfree radial point interpolation method (RPIM) for three dimensional solids. *Comput. Mech*. **36**, 421-430.

[15] Liu G.R., Gu, Y.T. (2001). A local point interpolation method for stress analysis of two-dimensional solids. *Struct. Eng. Mech.*, **11**(2), 221–236.

[16] Liu G.R., Gu Y.T. (2001). On formulation and application of local point interpolation methods for computational mechanics, *Proceedings of 1st Asia-Pacific Congress on Computational Mechanics*: Sydney, Australia, November 20–23, 97–106

[17] Bozkurt O.Y., Kanber B. and Asik M. Z. (2013). Assessment of RPIM shape parameters for solution accuracy of 2d geometrically nonlinear problems. *Int. J. of Comp. Meth.*, **10**(3), 1–26.

[18] Kanber B., Bozkurt O.Y. and Erklig A. (2013). Investigation of RPIM Shape Parameter effects on the Solution Accuracy of 2D Elastoplastic Problems. *Int. J. for Comp. Meth. in Engnrg. Science and Mechanics,* **14**(4), 354–366.

[19] Monaghan J.J., Gingold R.A. (1977). Smooth particle hydrodynamics: Theory and applications to non-spherical stars. *Man. Not. Roy. Astron. Soc.*, **181**, 378-389.

[20] Benz W. (1988). Applications of smoothed particle hydrodynamics (SPH) to astrophysical problems. *Comput. Phys. Comm.*, **48**, 97-105.

[21] Swegle J.W., Attaway S.W. (1995). On the feasibility of using smoothed particle hydrodynamics for underwater explosion calculations. *Comput. Mech.*, **17**, 151–168.

[22] Morris J.P, Fox P.J, Zhu Y. (1997). Modeling low Reynolds number incompressible flows using SPH. *J. Comput. Phys.*, **136** (1), 214– 226.

[23] Libersky L.D, Petscheck A.G (1991). Smoothed particle hydrodynamics with strength of materials. *Proceedings of the Next Free Lagrange Conference*, Springer-Verlag: New York, **395**, 248–257.

[24] Libersky L.D, Petscheck A.G (1993). High strain Lagrangian hydrodynamics- A three-dimensional SPH code for dynamic material response. *J. Comput. Phys*., **109**, 67–75.

[25] Johnson G.R, Beissel S. R. (1996). Normalized smoothing functions for SPH impact computations. *Int. J. Numerical Methods Eng.*, **39**(16), 2725–2741.

[26] Johnson G.R., Stryk R.A. and Beissel S.R. (1996). SPH for high velocity impact computations. *Comput. Methods Appl. Mech. Eng.*, **139**, 347–373.

[27] Altomore C. et al (2015). Applicabilty of smoothed particle hydrodynamics for estimation of sea wave impact on coastal structures. *Coastal Engineering*, **96**, 1-12.

[28] Benz W., Asphaug E. (1993). Explicit 3D continuum fracture modeling with smoothed particle hydrodynamics. *Proceedings of 24th Lunar and Planetary Science Conference*. Lunar and Planetary Institute, Houston, TX, 99–100.

[29] Sticko S. (2013). Smoothed particle hydrodynamics applied to fracture mechanics. Uppsala University, *UPTEC* F13 026.

[30] Bonet J., Kulasegaram S. (2000). Correction and stabilization of smoothed particle hydrodynamics methods with applications in metal forming simulations. *Int. J. Numerical Methods Eng.*, **47**, 1189–1214.

[31] Cleary P.W, Prakash M., Ha J. (2006). Novel applications of smoothed particle hydrodynamics (SPH) in metal forming. *Journal of Mat.Procssng.Tech.,* **177**, 41-48.

[32] Wang X.,Zheng Y., Liu H., Shen Z., Hu Y, Li W., Gao Y. and Guo C. (2012). Numerical study of the mechanism of explosive/impact welding using smoothed particle hydrodynamics method. *Materials & Design*, **35**, 210-219.

[33] Benz W., Asphaug E. (1995). Simulations of brittle solids using smoothed particle hydrodynamics. *Comput. Phys. Commun.*, **87**, 253–265.

[34] Liu M.B., Liu G.R, Zong Z. and Lam K.Y. (2003). Smoothed particle hydrodynamics for numerical simulation of underwater explosions. *Computational Mechanics*, **30**(2), 106-118.

[35] Liu M.B., Liu G.R, Zong Z. and Lam K.Y. (2003). Computer simulation of the high explosive explosion using smoothed particle methodology. *Computers & Fluids*, **32**(3), 305-322.

[36] Liu M.B., Liu G.R and Lam K.Y. (2003). A one dimensional meshfree particle formulation for simulating shock waves. *Shock waves*, **13**(3), 201-211

[37] Liu M.B., Liu G.R and Lam K.Y. (2003). Meshfree particle simulation of the detonation process for high explosives in shaped charge unlined cavity configurations. *Shock Waves*, **12**(6), 509-520.

[38] Belytschko T., Lu Y.Y. and Gu L. (1994). Element-free Galerkin methods. *Int. J. Numer. Meth. Engrg.*, **37**, 229-256.

[39] Wu CH., Chiu K. (2011). RMVT-based meshless collocation and element-free Galerkin methods for the quasi-3D free vibration analysis of multilayered composite and FGM plates. *Composite Structures*, **93**, 1433–1448.

[40] Wu CH. et al. (2011). RMVT-based meshless collocation and element-free Galerkin methods for the quasi-3D analysis of multilayered composite and FGM plates. *Composite Structures*, **93**, 923–943.

[41] Liu, G. R, Chen, X. L. (2001). A Mesh-free Method for Static and Free Vibration Analyses of Thin Plates of Complicated Shape. *Journal of Sound and vibration*, **241**, 839-855.

[42] Beissel S, Belytschko T. (1996). Nodal integration of the element-free Galerkin method. *Computer Methods in Applied Mechanics and Engineering*, **139**, 49–74.

[43] Samimi S. and Pak A. (2012). Three-dimensional simulation of fully coupled hydro-mechanical behavior of saturated porous media using Element Free Galerkin (EFG) method. *Computers and Geotechnics*, **46**, 75–83.

[44] Atluri S. N. and Zhu, T. (1998). A new meshless local petrov-galerkin (mlpg) approach in computational mechanics. *Computational Mechanics,* **22**, 117–127.

[45] Batra, R.C. and Porfir, M. (2008). Analysis of rubber-like materials using meshless local Petrov–Galerkin (MLPG) method. *Wiley InterScience*, **24**, 1781-1804.

[46] Batra, R.C. and Ching, H.K. (2002). Analysis of Elastodynamic Deformations near a Crack/Notch Tip by the Meshless Local Petrov-Galerkin (MLPG). *Tech Science Press*, **3**(6), 717-730.

[47] Pendhari S.S, Kant T., Desai Y. (2015). 2D Stress Analysis of Functionally Graded Beam Under Static Loading Condition**.** *Advances in Structural Engineering*, Springer, **1**, 35- 42.

[48] Li Q. et al. (2003). Application of Meshless Local Petrov-Galerkin (MLPG) to Problems with Singularities, and Material Discontinuities in 3-D Elasticity. *Tech Science Press*, **4**(5), 571-585.

[49] Lin H., Atluri S.N. (2001). The Meshless Local Petrov-Galerkin (MLPG) Method for Solving Incompressible Navier-Stokes Equations. *Tech Science Press*, **2**(2), 117-142.

[50] Atluri S. N. and Shen S.H. (2002). The Meshless Local Petrov-Galerkin (MLPG) Method: A Simple & Less-costly Alternative to the Finite Element and Boundary Element Methods. *Tech Science Press*. **3**, 1.11-51.

[51] Owen D.R.J. and Hinton E. (1980). Finite Elements in Plasticity: Theory and Practice, pp. 121-144.

[52] Labuschagne A., Van Rensburg N.F.J. and Van der Merwe A.J. (2009). Comparison of linear beam theories. *Mathematical and Computer Modelling*. **49**, 20-30.

[53] Chen W.F. and Han D.J. (1988). Plasticity for Structural Engineers. Springer-Verlag New York Inc.

[54] Lee P.S. and McClure G. (2005). A general three-dimensional L-section beam finite element for elasto-plastic large deformation analysis. *Computers and Structures*. **84**, 215-229.

[55] Timoshenko S.P. (1921). On the correction for shear of the differential equation for transverse vibration of prismatic bars. *Philos Mag*. **41**, 744–6.

[56] Shazali A.M, Rahman K., El-Boghdadi M.H, Taher S.F, Baluch M.H. (1997). A CDM-based computational model for the Timoshenko beam. *Engineering Computations*. **14**, 1, 57 – 74.

[57] Hughest, J.R, Taylor R.L. and Kanoknukulchi S. (1977). A simple and efficient finite element for bending. *Int. J. Num. Meth. Engng.,* **11**, 1529-1543.

[58] Hoffman J.D. (2001). Numerical Methods for Engineers and Scientists. Marcel Dekker Inc-New York, **2**, 302- 306.

[59] Liu G.R, Zhang G.Y, Wang Y.Y., Zhong Z.H, Li G.Y and Han X. (2007). A Nodal Integration Technique for Meshfree Radial Point Interpolation Method (NI-RPIM). *Journal of Solid and Structures*. **44,** 3845- 3847.

[60] Kanber B., Doğan N. F. and Tuvfik O. M. (2013). İnce Kirişlerin Elastik Davranışlarının NİY ve RNİY Yöntemleri İle İncelenmesi. XVIII. ULUSAL MEKANİK KONGRESİ, 26 - 30 Ağustos 2013, Celal Bayar Üniversitesi, Manisa. 340 – 348.

[61] Kanber B., Doğan N. F. (2013). Comparison of PIM and RPIM solutions of elasto-plastic thick beams. Int. J. of Aerospace and Lightweight Strctrs. **3**, No.2, 241-251.